Cenozoic magmatism in the western Ross Embayment: Role of mantle plume versus plate dynamics in the development of the West Antarctic Rift System

Sergio Rocchi,[1] Pietro Armienti,[1] Massimo D'Orazio,[1] Sonia Tonarini,[2] Jan R. Wijbrans,[3] and Gianfranco Di Vincenzo[2]

Received 12 March 2001; revised 13 February 2002; accepted 18 March 2002; published 20 September 2002.

[1] Geochemical and chronological data for Cenozoic plutons and dikes from northern Victoria Land (Antarctica), were used to propose a tectonic-magmatic model for this portion of the West Antarctic Rift System (WARS). The seven major plutons are compositionally bimodal, with gabbroic and syenitic portions. Among the 180 studied dikes, most are 1 m thick and have alkali basalt-basanite-tephrite compositions, along with minor intermediate rocks. Trachytic-rhyolitic dikes (up to 50 m thick) are by far less common. The ^{40}Ar-^{39}Ar data for dikes indicate middle Eocene to early Oligocene ages, the oldest found to date for igneous activity throughout the WARS. The geochronological-structural framework provides evidence for coeval emplacement of dikes on two main NW-SE and N-S striking trends, whereas plutonic-subvolcanic activity occurred in adjacent crustal sectors at different times. Mafic dikes display major and trace element distribution typical of basalts from oceanic islands, such as high ratios of Nb and Ta to large ion lithophile and heavy rare earth elements, coupled with prominent negative K and Pb anomalies in the primitive mantle-normalized multielement diagrams. Initial isotopic compositions are within the ranges of 0.70299–0.70372 for $^{87}Sr/^{86}Sr$ and 4.2–6.3 for ε_{Nd}. These features are shared by younger Neogene lavas. Geochemical modeling for both mafic dikes and lavas indicates an enriched magma source characterized by a residual potassic hydrous phase, thus pointing out a mantle source nearly uniform throughout 50 m.y. Comparable geochemical signature are reported for the magma source of the other Cenozoic volcanic provinces of the WARS and the whole Antarctic Plate. The new data for the early igneous rocks of the rift put in evidence a chronologic-structural link between magmatic evolution, regional tectonics and plate dynamics which suggests a model for WARS magmatism that is alternative to current plume hypotheses. We propose that magma genesis and emplacement are related to reactivation of preexisting translithospheric faults, which promoted local decompression melting of an enriched mantle that was previously veined during the decompression episode associated with the amagmatic late Cretaceous extensional rift phase. *INDEX TERMS:* 8109 Tectonophysics: Continental tectonics—extensional (0905); 1040 Geochemistry: Isotopic composition/chemistry; 3640 Mineralogy and Petrology: Igneous petrology; 1035 Geochemistry: Geochronology; 9310 Information Related to Geographic Region: Antarctica; *KEYWORDS:* Antarctica, rift, magmatism, geochemistry, plume, geochronology

Citation: Rocchi, S., P. Armienti, M. D'Orazio, S. Tonarini, J. R. Wijbrans, and G. Di Vincenzo, Cenozoic magmatism in the western Ross Embayment: Role of mantle plume versus plate dynamics in the development of the West Antarctic Rift System, *J. Geophys. Res.*, *107*(B9), 2195, doi:10.1029/2001JB000515, 2002.

1. Introduction

[2] Major continental rifts are usually associated with either short-lived large igneous provinces of continental flood basalts, or long-lasting alkaline magmatic provinces such as the Basin and Range of North America and the East African Rift. In both conditions, a connection between lithospheric extension, mantle plumes and magmatism is commonly assumed. However, whereas extension is always supported by geological evidence, often the existence of a plume can only be inferred. Additionally, a paradox exists

[1]Dipartimento di Scienze della Terra, Università di Pisa, Pisa, Italy.
[2]Istituto di Geoscienze e Georisorse, Consiglio Nazionale delle Ricerche, Pisa, Italy.
[3]Department of Isotope Geochemistry, Vrije Universiteit, Amsterdam, Netherlands.

0148-0227/02/2001JB000515$09.00

between the circular symmetry expected for a plume stress-induced perturbation and the surface linear expression of rifts [*Tommasi and Vauchez*, 2001]. Thus, the question about the causal relationships between plumes and extension is matter of debate. Indeed, since the original proposals of *Wilson* [1963] and *Morgan* [1971], plume occurrence has been frequently postulated just on the basis of magma chemistry, and plume theory has been stretched to the point that at least in some instances simpler explanations can be found. This controversy should be addressed in an integrated geological framework, where the space-time evolution of magma composition can be compared to the tectonic-geodynamic evolution of the host and surrounding lithospheric plates. Such a historical approach to the problem is one of the most significant and original contributions of the Earth sciences to the scientific way of thinking [*Frodeman*, 1995].

[3] In this paper, these issues are dealt with by a chronological-geochemical study of a prime example of long-lasting magmatism associated with an extensive area of rifted crust in Antarctica, known as the West Antarctic Rift System (WARS) [*Behrendt et al.*, 1991]. The WARS is one of the Earth's major active continental extension zones that crosses Antarctica for more than 3000 km (Figure 1). The paucity of chronologic-chronostratigraphic markers hampered until recently the historical-structural approach to the evolution of WARS, the only known post-Jurassic rocks being glacial deposits, along with Miocene to Recent volcanic rocks. In this paper, we describe Eocene-Oligocene plutonic and subvolcanic alkalic rocks recently found in northern Victoria Land on the western rift shoulder that expand the time interval of known Cenozoic igneous rocks back to 48 Ma [*Tonarini et al.*, 1997]. The igneous activity, covering a time span of almost 50 m.y., offers the opportunity to reconstruct the long-term evolution of WARS activity. The geological, chronological and geochemical data, along with geochemical modeling, show that the mantle source of magmatism, when evaluated with respect to the amplitude of temporal and areal distribution of magmatism, was relatively uniform over a wide area and lengthy time. The geochemical features of magmas from northern Victoria Land are also compared with others from WARS and nearby volcanic provinces of the Antarctic Plate. A critical review of the role of mantle plume models in the development of WARS, along with the discussion of an integrated geochemical-tectonic-chronological framework led us to develop a model that relates magmatism primarily to the plate dynamics and stress history of the Antarctic region.

2. West Antarctic Rift System: Regional Setting and Tectonics

[4] The West Antarctic Rift System is marked by a topographic trough 750 to 1000 km wide and 3000 km long, running from near the Ellsworth-Whitmore Mountains to the Ross Embayment-northern Victoria Land (Figure 1) [*LeMasurier and Thomson*, 1990; *Behrendt et al.*, 1991, 1992]. The WARS is similar in size to the East African rift system and to the Basin and Range province of the western United States [*Tessensohn and Wörner*, 1991] and is geometrically asymmetric. The eastern flank in Marie Byrd Land is characterized by basin-and-range style of topography, with about 3 km of uplift in the central part [*LeMasurier and Rex*, 1989]. The opposite flank in northern Victoria Land (NVL) consists of the Transantarctic Mountains, the uplifted roots of the early Paleozoic Ross Orogen [*Stump*, 1995, and references therein].

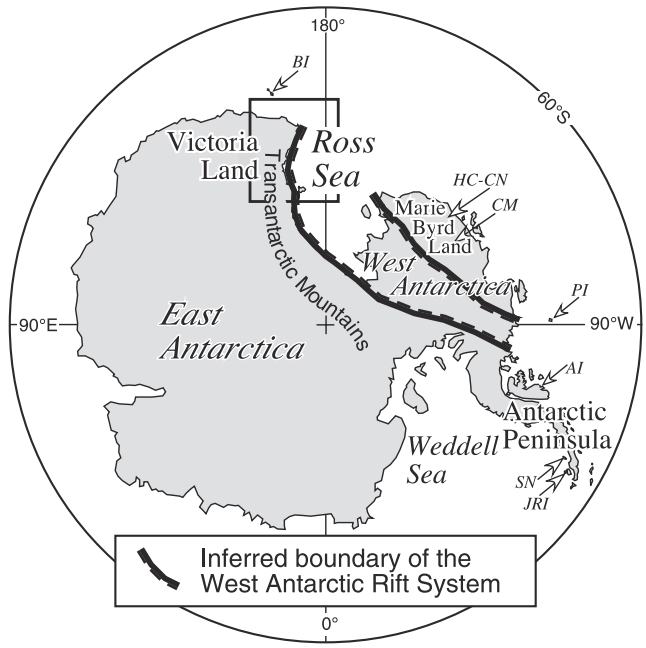

Figure 1. Sketch map of Antarctica showing the boundaries of the West Antarctic Rift System. Localities referred to in the text are also reported: Balleny Islands (BI), Peter I Øy (PI), Hobbs Coast and Coleman Nunatak of Marie Byrd Land (HC-CN), Crary Mountains of Marie Byrd Land (CM), Alexander Island (AI), Seal Nunataks (SN), James Ross Island (JRI). The box represents the area enlarged in Figure 2, the western Ross Embayment.

[5] During the Ross Orogeny, deep-reaching, NW-SE to NNW-SSE striking tectonic discontinuities were generated within the Transantarctic Mountains [*Gibson and Wright*, 1985; *Rocchi et al.*, 1998; *Finn et al.*, 1999]. Within the Devonian to Triassic time, the Ross Orogen was reduced by erosion to the Kukri Peneplain. Later, middle Jurassic magmatism and rifting affected NVL and East Antarctica, with generation of the Ferrar flood basalts, that were emplaced mainly along the backbone of the Ross Orogen [*Schmidt and Rowley*, 1986; *Storey and Alabaster*, 1991; *Elliot*, 1999]. This episode can be associated with the breakout of Africa-South America from Antarctica. During early Cretaceous, the Transantarctic Mountains were affected by amagmatic tectonics [*Fitzgerald and Stump*, 1997] while India and Australia were rifting away from Antarctica [*Stagg and Willcox*, 1992; *Chand et al.*, 2001].

[6] At late Cretaceous, a major phase of amagmatic rifting characterized the Ross Embayment, leading to local crustal thinning to the east of the Transantarctic Mountains and formation in the Ross Sea of four main N-S elongated basins, separated by basement highs. Widespread denudation occurred along the Transantarctic Mountains [*Stump and Fitzgerald*, 1992; *Balestrieri et al.*, 1994; *Fitzgerald*, 1994; *Fitzgerald and Stump*, 1997]. Contemporaneously, initial drifting between Australia and Antarctica occurred, with development of oceanic fracture zones as extensions of

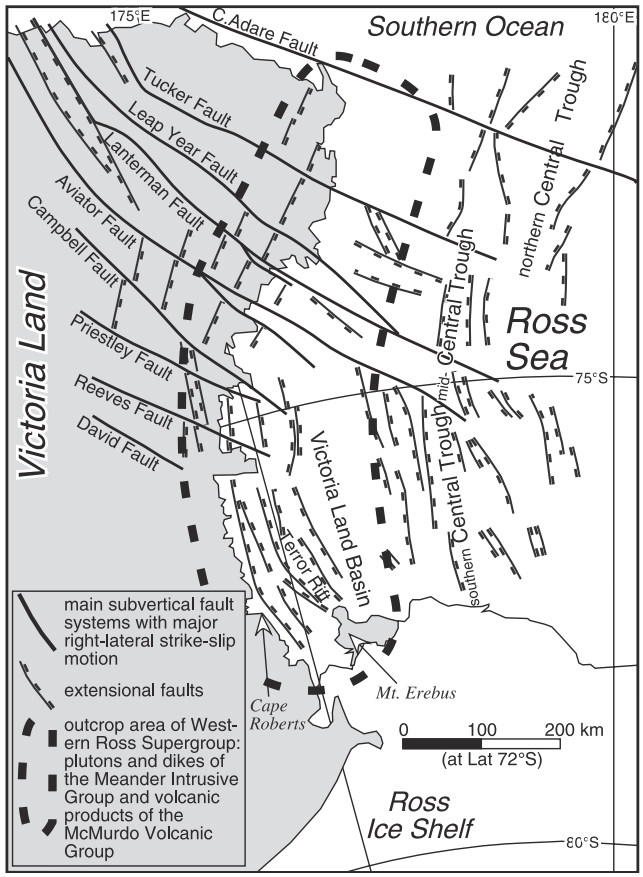

Figure 2. Structural-tectonic map of the western Ross Embayment, including Victoria Land and western Ross Sea area, redrawn after *Salvini et al.* [1997] and *Salvini and Storti* [1999].

major Paleozoic tectonic discontinuities of the Antarctic and Australian continents [*Foster and Gleadow*, 1992]. On the other side, the Campbell Plateau was breaking away from Marie Byrd Land and the Eastern Ross Sea margin, producing further tension on the Ross Sea crust.

[7] The early Cenozoic marked the inception of a major phase of denudation and rock uplift resulting in today's Transantarctic Mountains [*Fitzgerald and Stump*, 1997]. The concurrent amount of extension in the Ross Sea is a major issue in reconstructing the history of plate motion in the southwestern Pacific. The maximum late Cretaceous to Recent displacement between East and West Antarctica has been estimated by *Fitzgerald et al.* [1986] to be 255–350 km, while *Trey et al.* [1999] proposed 480–500 km, and *DiVenere et al.* [1994] suggested about 1000 km. For the Cenozoic magnitude of motion, a very low value (< 50 km) is proposed by *Lawver and Gahagan* [1994], while a higher value is regarded as possible by *Kamp and Fitzgerald* [1987], and 180 km of separation in the Western Ross Embayment in Eocene-Oligocene time has been suggested by *Cande et al.* [2000]. In northern Victoria Land, the movement was accommodated by NW-SE transtensional fault systems and N-S grabens and basins onshore and offshore, respectively (Figure 2) [*Salvini et al.*, 1997; *Salvini and Storti*, 1999].

[8] During the Cenozoic, widespread igneous activity affected the WARS. In northern Victoria Land, plutons, dike swarms, and volcanoes characterize an area of about 200 × 80 km. The volcanic products are part of the McMurdo Volcanic Group [*Kyle*, 1990], and the intrusive-subvolcanic rocks have been collectively named, in northern Victoria Land, the Meander Intrusive Group [*Müller et al.*, 1991; *Tonarini et al.*, 1997]. In this paper, we use the name Western Ross Supergroup to encompass the whole Cenozoic igneous province of the western rift shoulder (Figure 2).

3. Methods

[9] This study is based on some 200 rock samples from plutons and dikes cropping out in coastal northern Victoria Land between Campbell Glacier and Icebreaker Glacier. Sampling was carried out in conjunction with collection of structural data on dikes and mapping of pluton's exposures and internal variations. Petrographic data along with mineral chemistry, major and trace element data, Sr-Nd isotope compositions, and ^{40}Ar-^{39}Ar chronology were obtained on subsets of selected samples.

[10] Major elements were determined for 120 samples via XRF (Philips PW1480) on pressed powder pellets at the Dipartimento di Scienze della Terra, University of Pisa/CNR [*Franzini et al.*, 1975; *Leoni and Saitta*, 1976]. Na_2O, MgO, and K_2O were determined by atomic absorption spectrometry (AAS) and FeO by titration. Loss on ignition was determined by gravimetry at 1000°C after preheating at 110°C. Estimated uncertainties were generally better than 2% for major elements and better than 5% for concentrations >10 ppm for trace elements. The complete data set of major elements, along with 12 XRF trace elements and CIPW norms, are available as electronic supporting material[1] (Table A1).

[11] Trace elements were determined for selected samples by ICP-MS (Fisons PQ2 Plus®) at Dipartimento di Scienze della Terra, University of Pisa. Samples were dissolved in screw-top PFA vessels on a hotplate at ~120°C with HF-HNO_3 mixture. Analyses were performed by external calibration using basaltic geochemical reference samples as composition- and matrix-matching calibration solutions. The correction procedure includes (1) blank subtraction; (2) instrumental drift correction using Rh-Re-Bi internal standardization and repeated (every five samples) analysis of a drift monitor; (3) oxide-hydroxide interference correction. Precision, evaluated by replicate dissolutions and analyses of the in-house standard HE-1 (Mt. Etna hawaiite), is generally between 2 and 5% RSD, except for Gd (6%), Tm (7%), Pb and Sc (8%). Detection limits at 6σ level are in the range 0.002–0.02 ng mL^{-1} in the solution (corresponding to 0.002–0.02 ppm for a 1000-fold sample dilution) for all the elements, except for Ba, Pb, and Sr (0.1÷0.2).

[12] Sr and Nd isotopic compositions were determined using a Finnigan MAT 262V multicollector mass spectrometer following separation of Sr and Nd using conventional

[1] Supporting data tables are available via Web browser or via Anonymous FTP from ftp://agu.org, directory "apend" (Username= "anonymous", Password= "guest"); subdirectories in the ftp site are arranged by paper number. Information on searching and submitting electronic supplements is found at http://www.agu.org/pubs/esupp_about.html.

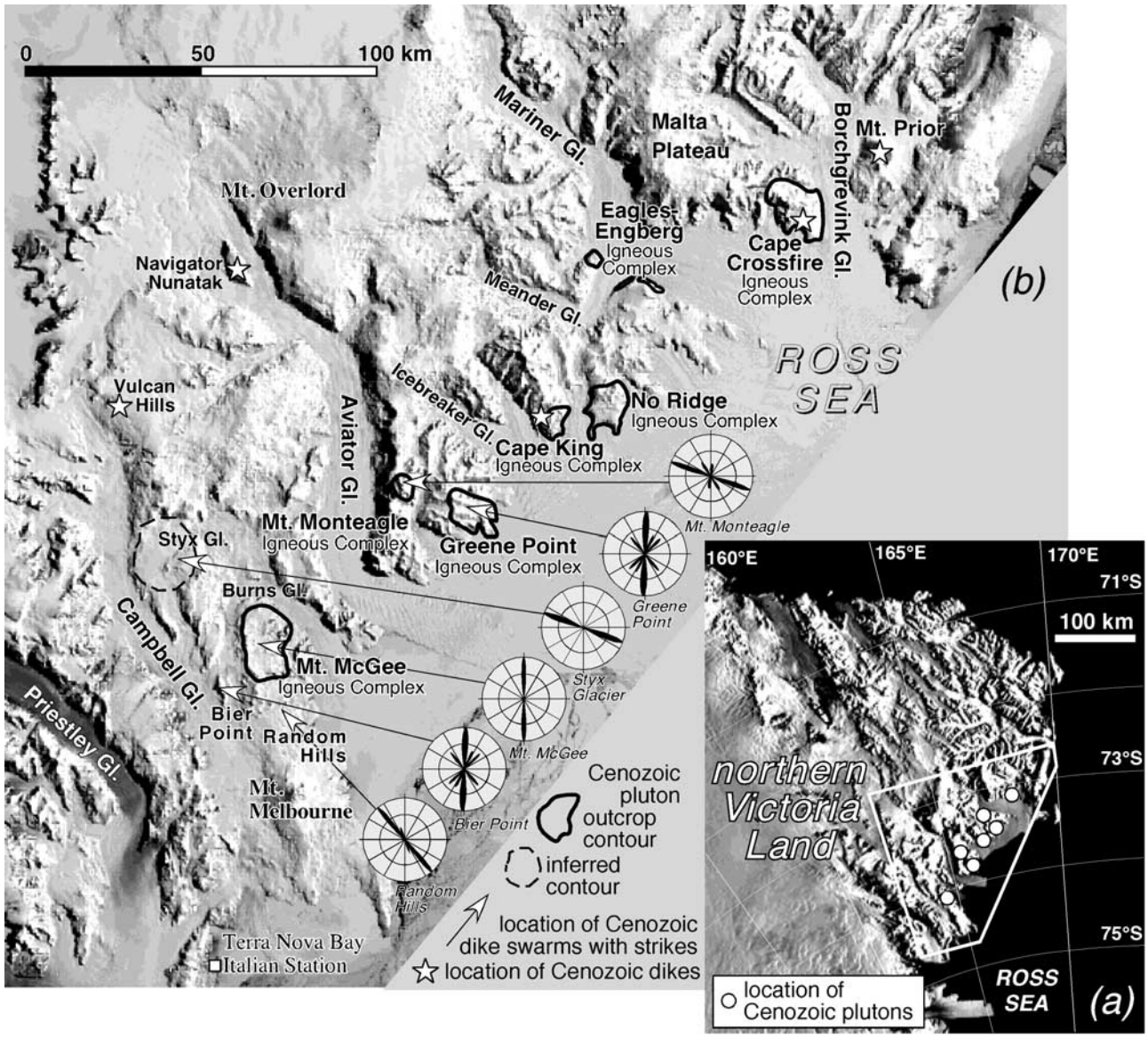

Figure 3. (a) Geographic map of northern Victoria Land, with location of the Cenozoic plutons along the Ross Sea coast. The polygon includes the area enlarged in Figure 3b. Base satellite image is taken from the Web page of the U.S. Geological Survey (http://TerraWeb.wr.usgs.gov/TRS/projects/Antarctica/). (b) Outcrop contours of the Cenozoic plutons, along with location and rose diagrams for strikes of the main dike swarms. Base image is a Landsat satellite image mosaic in Lambert conformal conic projection, courtesy of *Lucchitta et al.* [1987].

ion exchange procedures. Measured $^{87}Sr/^{86}Sr$ ratios have been normalized to $^{86}Sr/^{88}Sr = 0.1194$; $^{143}Nd/^{144}Nd$ ratios to $^{146}Nd/^{144}Nd = 0.7219$. During the course of this study, the average values obtained for NIST-SRM987 and La Jolla Nd standards are $^{87}Sr/^{86}Sr = 0.710250 \pm 5$ and $^{143}Nd/^{144}Nd = 0.511858 \pm 3$ (2σ mean, $n = 23$), respectively. The measured Nd isotopic ratios have been adjusted to $^{143}Nd/^{144}Nd = 0.511850$.

[13] Incremental laser heating ^{40}Ar-^{39}Ar ages were determined on nine amphibole separates from selected samples. Minerals were concentrated from grain size ranging from 100–150 to 250–350 μm using a Frantz Isodynamic separator and were carefully purified by handpicking under a binocular microscope, cleaned ultrasonically and dried with ultrapure acetone. The samples were irradiated for 12 h in the CLICIT facility at the Oregon State University TRIGA reactor along with the dating standard Taylor Creek Rhyolite sanidine [*Duffield and Dalrymple*, 1990]. The measurements were carried out at the Department of Isotope Geochemistry, Vrije Universiteit, Amsterdam. The experimental techniques are described in more detail by *Wijbrans et al.* [1995]. The laser power was increased from 0.3 to 0.8 W to melting over 13–18 steps, with the laser beam defocused to ~3 mm spot. System blanks were analyzed after every four sample extractions. Two samples (SA11b and XA2) were analyzed in duplicate. The full analytical results, corrected for interfering reactions from K and Ca, radioactive decay of ^{37}Ar and ^{39}Ar, mass spectrometer

Table 1. Summary of Petrographic Features of Cenozoic Plutons and Dikes From Northern Victoria Land[a]

Rock Type	Texture	Paragenesis	Alteration
		Greene Point Igneous Complex	
P gabbro-diorite	equigranular, medium-grained, hypidiomorphic	Plg, Aug, Bt, Ol (rare), Mag	rare Chl±Act
	cumulate (scattered)	Plg ± biotite	minor
P syenite	equigranular, coarse-grained, allotriomorphic	perth: Kfs, Na-Amph ± Na-Px±Fa	minor Kaol
	inequigranular, medium to fine grained, hypidiomorphic	perth: Kfs, Qtz, Na-Px ± Na-Amph	minor Kaol
D basanite-tephrite	aphanitic to slightly porphyritic (<5%)	pheno: Krs ± Ol ± Di; gm: Plg, Ne, Krs, Mag	(Cc,Ep,Chl, Act,Ser)
D mugearite-benmoreite-trachyte	porphyritic (10-20% large phenocrysts) or subaphyric	pheno: Plg, Krs ± Fa ± Anort; gm: Pl, Krs/Bt ± San	(Cc,Ep,Chl, Act,Ser)
D peralkaline trachyte	slightly porphyritic (5%, small phenocrysts)	*pheno*: San; *gm*: San, Aeg, Aenigm	Qtz + Kfs recrystallization
		Mount Monteagle Igneous Complex	
P gabbro	equigranular, medium-grained, hypidiomorphic	Plg, Aug, Hyp, Mag, Ilm	rare Chl ± Act
P syenite	equigranular, medium-fine-grained, hypidiomorphic, miarolitic	Kfs (perthite), Na-Px ± Aenigm	minor Kaol
D basanite-tephrite	slightly porphyritic (<5%)	pheno: Plg ± Ol (rare) ± large Krs; gm: Plg, Krs/Bt ± Ol ± Ne, Mag	(Cc, Ep, Chl, Act, Ser)
D benmoreite	aphyric, fine-grained, sometimes slightly hypocrystalline	gm: Plg, Krs/Bt, Hbl, Mag	(Cc, Ep, Chl, Act, Ser)
		Mt. McGee Igneous Complex	
P diorite	equigranular, medium to coarse-grained, hypidiomorphic	Plg, Aug, Bt, Hyp relics	minor
P monzonite-syenite	inequigranular allotriomorphic	large Kfs (perthite), Plg (in monzonites), Qtz, Hbl, Bt	minor
D basanite-hawaiite-mugearite	aphyric-subaphyric, sometimes slightly hypocrystalline	micropheno: Krs; gm: Plg ± San, Amph/Krs,Bt, Mag	(Cc,Ep,Chl, Act, Ser)
D trachyte	mainly aphyric to subaphyric	pheno: San or Anort; gm: Plg, San, Bt, Hbl ± Qtz, ±Mag	Qtz + Kfs recrystallization
		Random Hills Dike Swarm	
D alkaline basalt-hawaiite-tephrite	subaphyric	pheno: Ol, Krs; micropheno: Plg; gm: Plg, Krs, Magn ± Bt ± San	Cc, Ser±Chl±Act
		Bier Point Dike Swarm	
D alkaline basalt-hawaiite-tephrite	subaphyric	pheno: Ol, Krs; micropheno: Plg; gm: Plg, Krs, Magn ± Bt ± San	Cc, Ser±Chl±Act
D trachyte-rhyolite	aphyric to subaphyric	pheno: San or Anort ± Qtz (in rhyolites) ± Bt ± Na-Amph	gm silicified

[a] Abbreviations: P, plutonic rocks; D, dikes; Act, actinolite; Aeg, aegirine; Aenigm, aenigmatite; Amph, amphibole; Anort, anorthoclase; Aug, augite; Bt, biotite; Cc, carbonates; Chl, chlorite; Di, diopside; Ep, epidote; Fa, fayalitic olivine; Hbl, hornblende; Hyp, hyperstene; Ilm, ilmenite; Kaol, kaolinite; Kfs, K-feldspar; Krs, kaersutite; Na-Amph, eckermannite; Na-Px, aegirinaugite or aegirine; Ne, nepheline; Ol, forsteritic olivine; Mag, magnetite; Perth, perthitic; Plg, plagioclase; Qtz, quartz; San, sanidine; Ser, sericite; pheno, phenocrysts; gm, groundmass. Alteration mineral between parentheses are found in some samples of the group.

discrimination and blanks, are available as electronic supporting material (Table A2). A plateau is considered to be defined when ages recorded by three or more contiguous gas fractions which together comprise more than 50% of the total gas release, overlap at 2σ analytical error. The age steps do not include the uncertainty in the J value (estimated at 0.3%) that was, however, included in the calculated plateau and total fusion ages.

4. Results

4.1. Field and Petrographic Data

[14] The plutons of the Meander Intrusive Group are aligned along 200 km of the Ross Sea coast of NVL, on the elevated western rift shoulder between Campbell and Mariner Glaciers (Figures 3a and 3b), and usually have strong positive magnetic anomalies [*Müller et al.*, 1991]. The largest intrusions, Mt. McGee, Greene Point, No Ridge, and Cape Crossfire igneous complexes, each cover about 70–80 km^2 (Figure 3b). The intrusions of Mt. Monteagle, Cape King, and Eagles-Engberg Bluffs are smaller, with the best exposures on steep cliffs. All the intrusions have isotropic internal fabric, while the shape generally shows a weak elongation (≈1:1.7) striking around N140°E. Compositional zoning is common in the intrusions [*Tonarini et al.*, 1997], with mafic and felsic portions, sometimes interlayered and/or co-mingled [*Rocchi et al.*, 2002]. Mafic rocks are medium- to fine-grained equigranular gabbros and diorites and may show evidence of cumulus processes (for a summary of petrographic features, see Table 1). Syenites are generally equigranular, but grain size varies strongly among intrusions. Intermediate compositions are less common, occurring only in the McGee Igneous Complex.

[15] The dikes of Meander Intrusive Group total to at least 180 and occur as swarms cutting either the Paleozoic basement or the Cenozoic igneous complexes. These dikes

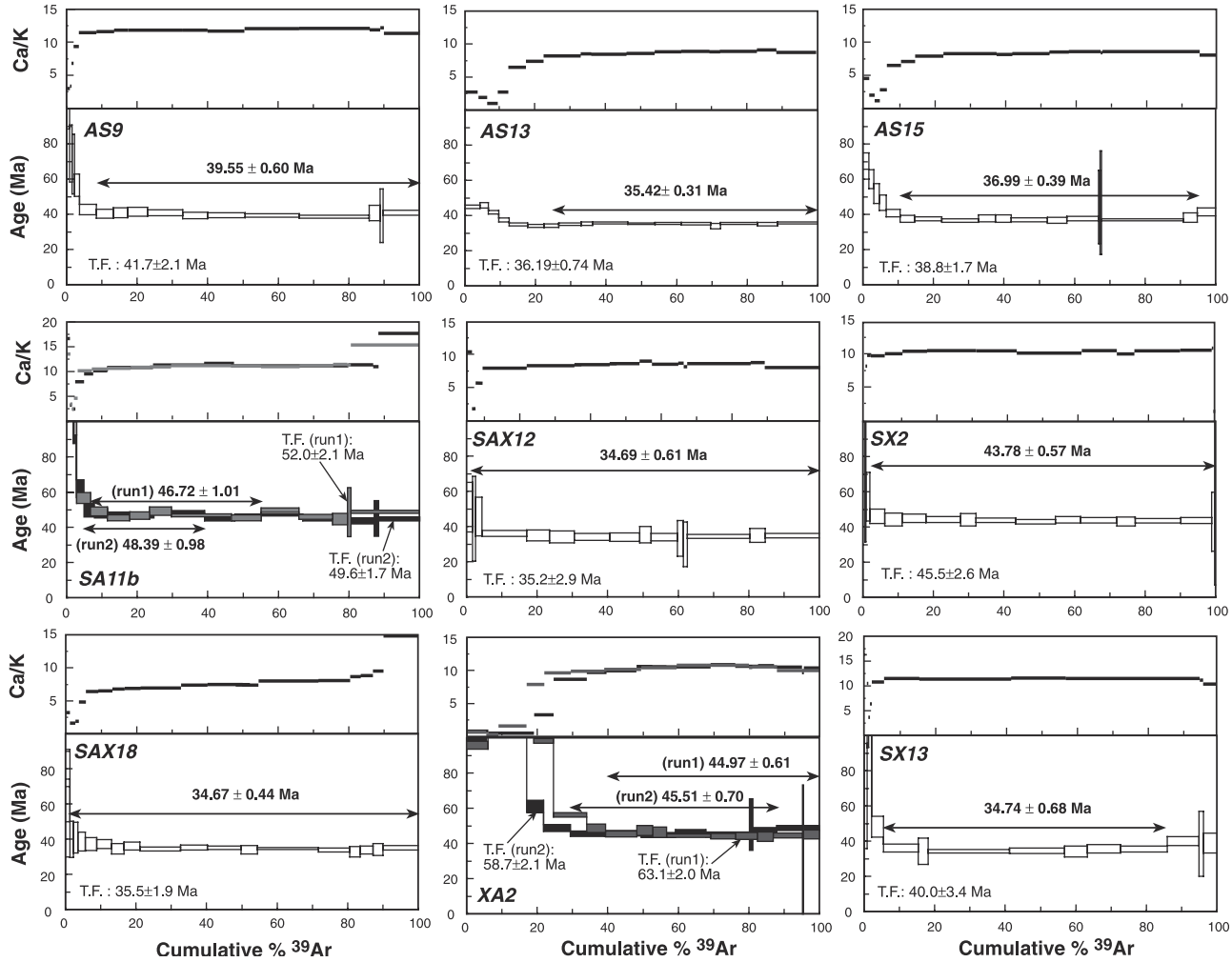

Figure 4. Age release and Ca/K spectra of amphibole fractions. Height of age boxes represents 2σ analytical error. Full analytical results are available as electronic supporting material.

are compositionally bimodal and strikes cluster around N-S or NNW-SSE (Figure 3b). The dikes cutting the Mt. McGee, Greene Point, and Mt. Monteagle igneous complexes have 17 measured strikes out of 25 clustered around N-S (Figure 3b). The McGee Igneous Complex is cut by 1 to 5 m thick dikes, with N-S orientation, subvertical dip, and sharp contacts against the host rock. The dikes cutting the Greene Point Igneous Complex have thicknesses of 1 to 5 m and are oriented around two main strikes: N0-45°E and N140°E. Interfaces between dikes and the host gabbro-syenite pluton are sometimes strongly lobate and grade into meter-sized enclave trains, while in other instances the dikes have sharp and rectilinear contacts against the host syenite. The dikes cutting the syenitic portion of Mt. Monteagle intrusion are about 10 m thick and strike around N110°E, whereas those cutting the gabbro are thinner (<1 m) and show N-S orientation (Figure 3b). All have sharp, rectilinear contacts against the host rock. Swarms of mafic, unweathered dikes cut the Paleozoic basement at Bier Point, Random Hills, Vulcan Hills, and Navigator Nunatak. Felsic deeply altered dikes crop out in the area between Styx and Burns Glaciers and at Navigator Nunatak. All the contacts with the host rock are rectilinear and sharp. The mafic dikes from Bier Point area are ≈1 m thick. The strikes are evenly distributed between N-S and NNW-SSE directions; sometimes N-S dikes cut N150°E dikes (Figure 3b). In the Random Hills area the mafic dikes are 1 m thick and almost all strike on NNW-SSE direction (Figure 3b). The mafic dikes have mainly alkali basalt-basanite-tephrite composition, with minor hawaiites and K-trachybasalt (Table 1). The felsic dikes have thicknesses ranging from 1 to about 50 m and do not show any preferred orientation. They are deeply weathered, unsuitable for geochemical investigation.

4.2. The ^{40}Ar-^{39}Ar Chronology

[16] New ^{40}Ar-^{39}Ar dates on kaersutite phenocrysts from dikes have been performed to better constrain the relationships between chronology and geographical distribution, attitude (N-S or NNW-SSE strike) and outcrop conditions (within the plutons or cutting the basement). A common feature of all age spectra (Figure 4) is that the first heating steps (commonly for less than 10% of the total ^{39}Ar released) are characterized by low and heterogeneous Ca/K ratios typical of amphibole intergrown with other K-rich mineral phases (phyllosilicates). These low-temper-

Table 2. Summary of Laser Incremental Heating Results on Kaersutite Phenocrysts From Cenozoic Dikes of Northern Victoria Land

Sample	Run	Locality	Rock Type	Total Fusion Age, Ma	Plateau Age, Ma	Steps[a]	^{39}Ar Plateau, %	Isochron Age[b]	Steps[c]	MSWD[d]	^{40}Ar/^{36}Ar Intercept	Preferred Age, Ma
2.11.93 SX13		Mt. McGee	hawaiite	40.0±3.4	34.74±0.68	6-12	80.4	no solution	5–15	-	-	34.74±0.68
2.11.93 SX2		Mt. Monteagle	tephrite	45.5±2.6	43.78±0.57	2–17	99.4	42.9±1.3	5–16	0.34	363±110	43.78±0.57
10.11.93 SAX12		Greene Point	trachybasalt	35.2±2.9	34.69±0.61	2–15	98.3	33.7±2.7	4–15	0.46	377±280	34.69±0.61
10.11.93 SAX18		Greene Point	basanite	35.5±1.8	34.67±0.44	2–18	98.8	32.5±1.7	5–17	0.44	390±76	34.67±0.44
1.11.93 AS9		Random Hills	latite	41.2±2.1	39.55±0.60	5–16	91.6	31±16	5–16	0.26	1058±1400	39.55±0.60
1.11.93 AS13		Random Hills	tephrite	36.19±0.74	35.42±0.31	7–17	77.6	36.53±0.50	7–17	0.52	195±41	35.42±0.31
1.11.93 AS15		Random Hills	basanite	38.7±1.7	36.99±0.39	6–17	84.2	36.0±2.2	7–18	0.54	409±290	36.99±0.39
8.11.93 SA11b	1	Bier Point	alkali basalt	52.0±2.1	46.7±1.0	6–11	48.4	40.7±5.1	5–16	0.56	1103±610	39.9±4.2[e]
	2			49.6±1.7	48.39±0.98	5–9	34.1	38.4±7.2	5–15	0.77	1256±850	
4.11.93 XA2	1	Bier Point	hawaiite	63.1±2.0	44.97±0.61	7–16	60.6	44.0±3.4	5–16	2.1	379±380	45.20±0.46[f]
	2			58.7±2.1	45.51±0.70	6–12	58.5	29±28	4–13	0.29	2038±2700	

[a] Heating steps included in the plateau.
[b] The x intercept in a ^{36}Ar/^{40}Ar versus ^{39}Ar/^{40}Ar isochron plot using the heating steps yielding Ca/K ratios expected for analyzed kearsutites.
[c] Heating steps included in the regression calculation.
[d] MSWD, mean square weighted deviation.
[e] Weighted mean of the isochron ages from run 1 and run 2.
[f] Weighted mean of the plateau ages from run 1 and run 2.

ature steps yield ages more or less significantly older than the remaining portion of the age profile (Figure 4), possibly suggesting the presence of a minor excess argon component. Most of the analyzed amphiboles yield statistically valid plateau ages between ~35 and 45 Ma (Figure 4). There is a general agreement, within error limits, between the plateau and total fusion ages. However, some samples, especially XA2, have total fusion ages significantly older than the plateau ages suggesting a more important contamination by the excess component. Sample SA11b does not yield a statistically valid plateau. However, six contiguous steps in run 1 (~48% of the released $^{39}Ar_{(K)}$) and five in run 2 (~34% of the released $^{39}Ar_{(K)}$), yield ages overlapping, within error limits, at ~47 Ma. Least squares fits in a $^{36}Ar/^{40}Ar$ versus $^{39}Ar_{(K)}/^{40}Ar$ isochron diagram were calculated for all amphibole analyzed using the heating steps which, based on the Ca/K ratios (derived from the measured $^{37}Ar_{(Ca)}/^{39}Ar_{(K)}$ ratios), may confidently be referred to degassing of amphibole. The results of the regression calculations along with total fusion, plateau ages and the selected amphibole ages for all mineral samples are summarized in Table 2. Note that in the studied samples, the effectiveness of the isochron approach is limited by the high radiogenic content (generally >90%) of most of the heating steps and by the scarce spread of the data points in the isochron diagram. This causes poorly constrained regression lines yielding intercepts with high uncertainties. From Table 2 it is evident that only for sample SA11b, the regression calculations gave initial $^{40}Ar/^{36}Ar$ ratios statistically higher than modern atmospheric argon and intercept ages younger than the near-plateau dates. K-Ar amphibole ages are usually interpreted to record cooling below ~550°C even though natural examples in which amphibole registered crystallization ages are not uncommon. However, the rapid cooling experienced by the studied dikes, as testified by the porphyritic texture with very fine-grained groundmass, ensures that amphibole ages approach the emplacement time of the dikes.

[17] These data expand the chronologic framework for Cenozoic magmatism of NVL based on the K-Ar dates of *Müller et al.* [1991] and the Rb-Sr whole rock-biotite dates of *Tonarini et al.* [1997]. The main pieces of evidence from the chronologic framework are summarized in Figure 5. The ages of the NVL plutons range from 48 to 23 Ma, while the ages of the dikes range from 46.7 to 34.7, with a felsic dike from Mt. Prior dated at 18 Ma (Figure 5a). The dikes with lobate contacts towards the host gabbro-syenite (Greene Point Igneous Complex) have Rb-Sr whole rock-biotite ages (40–39 Ma) covering the younger end of the host intrusion age (48–39 Ma). The dikes cutting the plutons with sharp rectilinear contacts were found in all the studied plutons and their amphibole ^{40}Ar-^{39}Ar ages are a few million years younger than the host intrusion. Thus the plutonic and subvolcanic activity overlap in time, with the age of the whole plutonic-subvolcanic association ranging from 48 to 18 Ma. The dikes cutting the plutons were emplaced between 44 and 35 Ma, while the dikes cutting the Paleozoic basement have amphibole ^{40}Ar-^{39}Ar ages ranging from 46 to 35 Ma (Figure 5b). No significant age difference can be detected between the two modes of dike occurrences. The age range for NNW-SSE dikes is 45.0–35.4 Ma, while N-S dikes were emplaced from 46.7

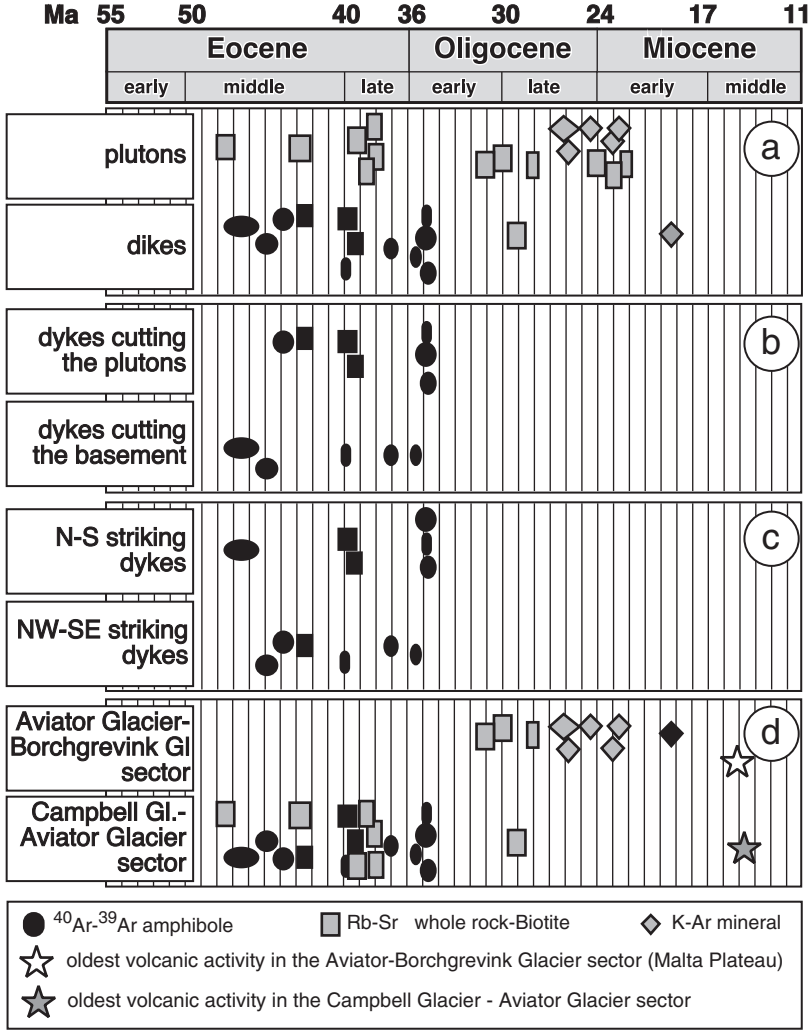

Figure 5. Chronologic framework of Cenozoic igneous activity in northern Victoria Land. Data sources are for ^{40}Ar-^{39}Ar, this work; Rb-Sr whole rock-biotite, *Müller et al.* [1991], *Tonarini et al.* [1997], and *Rocchi et al.* [2002]; and K-Ar on minerals, *Müller et al.* [1991]. The width of symbols is proportional to the analytical error. The 29 Ma date reported by *Tonarini et al.* [1997] for a syenitic dike from Styx Glacier (Campbell-Icebreaker Glaciers sector) has to be regarded with caution, owing to the textural and mineralogical evidence for secondary recrystallization coupled with a anomalously high initial Sr isotopic ratio.

to 34.7 Ma (Figure 5c). At Bier point (where crosscutting relationships between dikes with different orientation have been observed) the amphibole ^{40}Ar-^{39}Ar age of a N30°E dike and a N140°E dike are 46.7 ± 1.0 and 45.7 ± 0.6 Ma, respectively. Thus emplacement of magma was contemporaneous for the two main trends. In the area between Campbell Glacier and Icebreaker Glaciers the igneous activity (plutons and dike swarms) is restricted to the time interval 48–29 Ma, whereas between Icebreaker and Borchgrevink Glaciers the magmatism has been active between 31 and 18 Ma (Figure 5d). In the area between Campbell and Icebreaker Glaciers the plutonic-subvolcanic activity is separated from the volcanic activity by a time gap of about 14 m.y. (see *Armienti and Baroni* [1999] for a review). By contrast, north of Icebreaker Glacier, no significant time gap exists between the youngest plutonic-subvolcanic activity and the oldest volcanic rocks from the Malta Plateau (Figure 5d). In southern Victoria Land the oldest isotopically dated magmatic products (24.22 ± 0.06 Ma [*Cape Roberts Science Team*, 1999] are tephra layers from a core off Cape Roberts. The age of oldest dated outcrop of volcanic rocks is 19 Ma [*Kyle and Muncy*, 1989], and volcanism has been continuous since then to the present.

4.3. Geochemistry

[18] The plutonic rocks show a mainly gabbro-syenite bimodal distribution (Table 1, supporting material Table A1, and Figure 6). The least evolved intrusive rocks are often *ol-hy* normative and mildly alkaline, whereas syenites are generally *Q*-normative, sometimes peralkaline (Greene Point). Most dikes are basic to intermediate in composition, bridging the SiO_2 gap found for the intrusive rocks. The whole dike association is alkaline to strongly alkaline

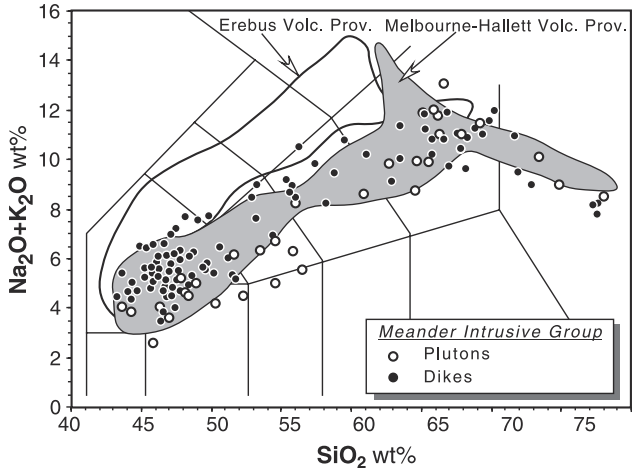

Figure 6. TAS diagrams [*Le Bas et al.*, 1986] for the studied plutonic-subvolcanic association. Volcanic products from the Melbourne and Hallett Volcanic Provinces [*LeMasurier and Thomson*, 1990; *Armienti et al.*, 1991] and the Erebus Volcanic Province [*LeMasurier and Thomson*, 1990; *Kyle et al.*, 1992] are reported for comparison.

(Figure 6), and is generally *ne*-normative. The overall compositional spectrum of the plutons and dikes from the Meander Intrusive Group (Figure 6) matches that of the geographically overlapping Melbourne Volcanic Province [*LeMasurier and Thomson*, 1990; *Armienti et al.*, 1991], which however also contains scarce phonolites; the compositions of the southernmost Erebus Volcanic Province are more alkali-enriched and strongly silica undersaturated [*Kyle et al.*, 1992].

[19] The trace element distribution has been used to investigate the nature of the mantle magma source. In Tables 3 and 4, geochemical data selected mafic samples from plutonic-subvolcanic Meander Intrusive Group are reported. The trace element contents of plutonic rocks are commonly not representative of a melt, nonetheless some features are distinguishable. The chondrite-normalized distribution of rare earth elements (REE) of gabbros are roughly rectilinear and light REE (LREE)-enriched ($La_N \approx 100-300$), with La_N/Yb_N variable between 11.2 and 19.0. Moderate positive Eu anomalies (Eu/Eu* up to 1.5) are always present coupled with the petrographic evidence of cumulus plagioclase, such as tiling of plagioclase laths. The overall distribution of incompatible elements is dominated by high ratios of Nb-Ta to large ion lithophile elements (LILE) and Y-heavy REE (HREE), and by high primitive mantle-normalized La/K (1.0–4.5).

[20] Mafic dikes are always subaphyric or slightly porphyritic; thus they are suitable representatives of magmatic liquids. They display rectilinear chondrite-normalized REE patterns with strong LREE-enrichment ($La_N \approx 200-400$), and rare moderate positive Eu anomalies. La_N/Yb_N varies from 12.1 to 22.6 and is roughly positively correlated with fractionation of LREE (La_N/Sm_N = 2.4–4.1) and HREE (Tb_N/Yb_N = 2.1–3.7) and with La_N and ΣREE_N. The distribution of incompatible elements is dominated by high ratios of Nb and Ta to LILE and Y-HREE, as is typical of ocean island basalts (OIB) [*Sun and McDonough*, 1989] (Figure 7). Noticable are the ubiquitous, prominent negative K and Pb anomalies. The overall trace element distribution does not show significant differences between intrusive rocks and dikes. Neogene volcanic rocks from NVL display a comparable trace element distribution, with even more marked negative K and Pb anomalies (Figure 7).

[21] The $^{87}Sr/^{86}Sr$ (t) ratios for whole rock samples varies from 0.70299 to 0.71297 (Table 5), and ε_{Nd}(t) is between 2.0 and 6.3. However, some samples could be affected by fractional crystallization coupled with host rock assimilation [*Tonarini et al.*, 1997]. Therefore we discarded samples with either Sr < 600 ppm or Sr and Nd isotope ratios significantly shifted towards the average composition of granitoid basement [*Rocchi et al.*, 1998]. The screened data set shows initial isotopic ratios in the more restricted range of 0.70299–0.70372 for $^{87}Sr/^{86}Sr$ and of 0.512941–0.512839 for $^{143}Nd/^{144}Nd$(t), corresponding to ε_{Nd}(t) between 6.3 and 4.2. All the data plot in the depleted quadrant of the plane $\varepsilon_{Nd}-^{87}Sr/^{86}Sr$, where they define a rough negative correlation (Figure 8). Sr-Nd isotope compositions of plutons and dikes range across the same interval as younger Neogene lavas, although data for dikes and plutons cluster towards slightly more enriched compositions with respect to younger lavas. The overall difference of isotopic ratios between the plutonic-subvolcanic association (48–29 Ma) and the volcanic products (<15 Ma) cannot be ascribed to the age difference between the two groups. Indeed, if two distinct batches of magmas were extracted from a common source (with Rb/Sr and Sm/Nd typical of OIB sources) at 48 Ma and today, respectively, they should differ by 0.30 ε_{Nd} units and 0.000021 $^{87}Sr/^{86}Sr$ units. These values are within twice the typical error on both Sr and Nd measured isotopic ratios (Table 5) and are therefore neglected.

5. Discussion of Data

5.1. Geochemical Modeling of NVL Magma Source

[22] The variations in incompatible element ratios for mafic dikes are very restricted, with an overall OIB-type distribution of trace elements that is shared by all the dike samples. The nearly uniform trace element and isotope features of the whole dike association is compatible with an origin by variable degrees of melting of an approximately homogeneous source. In the attempt to model the composition of the mantle magma source, we selected out from Tables 3 and 4 only dike samples with MgO > 6 wt %. In order to test the validity of this choice, we show that the ranges of La/Nb (always <0.80) and Ba/Nb do not change when different thresholds (MgO > 6 wt %, MgO > 4 wt %) are considered (Figure 9): this lends further support to the pristine origin of these ratios, and the value of MgO = 6 wt % is considered as a robust threshold for the data set to be used in source modeling. We used the same modeling techniques as *Hart et al.* [1997], i.e., the inverse approach of *Minster and Allègre* [1978] with the formulations of *Sims and DePaolo* [1997]. The assumptions of the model are that (1) the incompatible elements ratios in the selected samples only depend on the source composition and melting process, (2) the magma source is unique, and (3) the magma was generated by a modal batch melting process. The trace

Table 3. Representative Major and Trace Element Analyses of Mafic Intrusive Rocks and Mafic Dikes Cutting Plutons

	Greene Point Igneous Complex							Mt. Monteagle Igneous Complex			McGee Igneous Complex			
	Intrusive Rocks		Dikes					Intrusives	Dikes		Intrusives	Dikes		
	21–10–93 A1c Gabbro	21–10–93 A1d Gabbro	10–11–93 SAX21 Gabbro	10.11.93 SAX22 Basanite	10.11.93 SAX11 Alkaline Basalt	10.11.93 SAX12 K-Trachyb	10.11.93 SAX18 Basanite	2.11.93 SX10b Gabbro	2.11.93 SX4 Basanite	2.11.93 SX9 Basanite	19.1.91 LZ42 Qtz Diorite	2.11.93 SX13 Hawaiite	2.11.93 SX17 K-Trachyb	2.11.93 SX18 K-Trachyb
Major Elements, wt %														
SiO_2	46.09	45.44	47.03	42.33	45.06	45.30	47.20	44.90	42.82	42.30	53.22	46.94	48.32	48.19
TiO_2	3.48	4.14	3.04	4.48	3.36	3.62	3.45	5.07	3.73	3.45	2.08	2.83	3.32	3.14
Al_2O_3	17.23	16.02	17.92	15.42	14.19	14.84	14.41	14.79	13.07	12.61	19.01	15.16	14.99	15.12
Fe_2O_3	2.66	6.66	2.58	3.51	4.45	4.69	3.84	3.00	6.95	3.81	1.88	3.28	3.50	4.02
FeO	9.61	6.44	8.42	11.00	8.86	7.75	6.99	11.21	7.28	9.40	6.75	7.48	8.03	7.50
MnO	0.24	0.23	0.16	0.22	0.21	0.19	0.19	0.21	0.18	0.25	0.18	0.17	0.16	0.14
MgO	4.77	5.04	3.67	6.15	7.28	4.70	6.28	7.30	6.88	9.39	2.59	4.26	6.76	6.33
CaO	9.21	9.12	9.57	9.08	8.07	8.25	7.21	8.94	8.08	8.83	7.23	6.74	7.01	6.82
Na_2O	3.04	3.03	3.96	3.35	3.16	3.78	4.75	1.98	3.97	2.67	3.71	4.30	3.58	3.47
K_2O	0.55	0.95	0.64	0.64	1.63	1.97	2.17	0.67	2.38	2.16	1.20	1.78	1.90	1.76
P_2O_5	1.90	1.85	1.53	1.32	1.02	1.17	0.89	0.67	0.81	0.77	1.07	0.85	0.83	0.72
LOI	1.23	1.07	1.48	2.50	2.70	3.73	2.62	1.26	3.85	4.37	1.09	6.22	1.61	2.77
Trace Elements, ppm														
Sc	16	19	15	17	19	15	16	25	19	20	17	13	16	14
V	81	168	80	232	209	179	184	337	207	214	69	138	177	164
Cr	0.2	1.4		10	181	8	139	4	153	247	1.6	34	59	57
Co	24	26	22	41	40	31	38	46	41	47	15	32	38	35
Ni	5	9	4	18	103	12	122	10	117	235	7	51	58	56
Cu		43		50	46	48	44		73				48	
Rb	8.8	16.9	13.4	4.9	47	60	59	21.1	67	57	36	39	43	44
Sr	1358	1161	1521	1258	937	1049	1274	762	843	670	1293	840	736	706
Y	36	48	24.3	32	26.6	43	43	23.5	32	26.9	28.7	32	29.3	27.2
Zr	65	134	64	120	212	511	573	126	399	295	46	359	311	331
Nb	40	67	24.7	63	60	108	133	44	87	63	44	68	59	60
Mo	1.6	2.0	1.8	1.3	1.2	5.4	6.2	1.5	4.5	3.8	2.1	3.7	3.2	0.5
Cs	0.11	0.14	0.20	0.06	1.11	1.27	5.5	0.52	6.2	5.3	1.41	1.60	1.62	1.61
Ba	577	733	388	429	545	690	703	245	453	394	2318	480	467	649
La	55	66	41	51	43	82	97	24.8	58	47	49	55	45	47
Ce	119	146	86	108	87	167	191	55	119	95	101	111	95	96
Pr	15.9	19.9	11.2	13.6	10.3	19.7	21.8	7.1	14.5	11.7	12.9	13.7	11.9	12.0
Nd	68	86	48	58	42	76	83	31	56	47	53	53	49	49
Sm	13.5	17.2	9.5	11.5	8.4	14.2	14.8	6.7	11.3	9.4	10.3	10.1	10.4	10.2
Eu	5.4	6.4	4.2	3.9	2.86	4.2	4.4	2.34	3.3	2.86	7.2	3.1	3.1	3.15
Gd	10.7	12.9	7.3	8.9	6.6	10.6	11.0	5.4	8.8	7.4	9.2	8.1	8.3	8.0
Tb	1.51	2.01	1.04	1.27	1.02	1.65	1.66	0.84	1.37	1.11	1.12	1.20	1.32	1.19
Dy	7.8	10.3	5.1	6.7	5.2	8.5	8.7	4.6	6.9	6.0	5.8	6.5	6.4	6.3
Ho	1.38	1.84	0.92	1.20	0.96	1.60	1.59	0.87	1.24	1.01	1.04	1.18	1.11	1.05
Er	3.0	4.1	1.98	2.76	2.26	3.8	3.8	2.00	2.82	2.29	2.41	2.83	2.52	2.31
Tm	0.35	0.50	0.23	0.35	0.31	0.53	0.50	0.23	0.39	0.27	0.29	0.35	0.33	0.26
Yb	1.96	2.88	1.32	2.06	1.84	3.2	2.92	1.50	2.20	1.73	1.70	2.28	1.94	1.57
Lu	0.28	0.35	0.19	0.30	0.27	0.45	0.43	0.21	0.26	0.26	0.25	0.32	0.24	0.23
Hf	2.38	4.2	2.13	3.7	4.4	10.9	12.6		8.7	7.0		8.1	6.6	
Ta	2.78	4.0	1.93	4.1	3.8	7.1	8.6	3.1	5.9	4.1	2.84	4.5	3.9	4.1
Pb	1.0	1.6	2.0	1.5		5.2	6.2	2.5	5.9		5.9	3.3	3.7	10.4
Th	1.97	2.89	2.91	1.95	4.5	9.8	12.6	2.30	8.2	5.6	4.4	6.5	4.9	5.3
U	0.47	0.83	0.73	0.50	1.31	2.80	3.1	0.47	2.63	1.56	0.75	1.81	1.31	1.37

element distribution of the source depends on the choice of a reference concentration for an element in the source. We chose to fix the concentration of dysprosium at 0.5 × primitive mantle value [*McDonough and Sun*, 1995], taking into account the relative constancy of HREE in peridotites and to better compare our results with those obtained by *Hart et al.* [1997] for the source of Marie Byrd Land lavas. The resulting spidergram of the source (Figure 10) clearly shows the enriched nature of the mantle source of NVL magmas, and this is a robust feature independent of the choice of the reference value (of Dy). The low La/Nb and Ba/Nb are evidence for a lack of significant contribution from subduction–modified continental lithosphere.

[23] The source modeling for dike magmatism also yields bulk solid-liquid partition coefficients which can be used to make deduction about the source mineralogy: The obtained partition coefficient for K is relatively high and can be ascribed to the occurrence of a residual potassic phase in the source. This is also supported by investigations of the relative enrichments of trace elements (enrichment ratio), which depends on bulk partition coefficients, and can thus be used as a probe to source mineralogy, following the approach of *Class and Goldstein*

Table 4. Representative Major and Trace Element Analyses of Mafic Dikes Cutting Crystalline Basement

	Random Hills Dike Swarm												Bier Point Dike Swarm			
	1.11.93 AS1 Alkaline Basalt	1.11.93 AS2 Basanite	1.11.93 AS3 Hawaiite	1.11.93 AS5 K-Trachyb	1.11.93 AS11 Basanite	1.11.93 AS12 th. Basalt	1.11.93 AS13 Tephrite	1.11.93 AS14 Phonoteph	1.11.93 AS15 Basanite	1.11.93 AS16 Basanite	1.11.93 AS18 Tephrite	1.11.93 AS19 Tephrite	4.11.93 XA1 Basanite	4.11.93 XA2 Hawaiite	4.11.93 XA3 Hawaiite	4.11.93 XA14 Basanite
Major Elements, wt %																
SiO_2	46.47	44.57	44.02	44.86	43.07	44.10	44.79	46.76	43.72	43.97	44.91	45.61	45.36	46.08	45.11	42.78
TiO_2	2.77	3.14	3.99	3.27	4.26	4.22	3.72	2.61	4.15	3.28	3.45	3.20	3.72	3.43	3.67	4.15
Al_2O_3	16.28	13.71	14.10	15.49	13.95	13.87	14.81	14.31	14.36	13.81	14.99	15.28	14.86	14.83	14.86	14.29
Fe_2O_3	1.51	3.66	2.47	2.50	2.91	2.50	3.43	2.93	3.14	3.53	3.89	3.46	3.33	2.76	3.81	4.06
FeO	9.61	9.28	10.02	9.00	9.91	9.85	8.80	8.74	10.01	9.06	8.62	8.37	10.28	9.80	9.80	9.68
MnO	0.17	0.18	0.18	0.16	0.17	0.17	0.16	0.18	0.16	0.17	0.15	0.15	0.20	0.16	0.15	0.16
MgO	8.28	6.16	6.36	5.02	5.84	5.35	4.32	4.28	5.44	6.77	4.14	3.59	4.67	4.56	4.37	7.37
CaO	8.95	8.06	8.29	8.47	8.35	9.41	7.26	6.92	8.03	8.80	7.83	7.58	7.93	7.24	6.67	8.26
Na_2O	3.44	4.63	3.36	3.39	4.08	3.10	4.67	5.12	4.33	4.14	4.94	5.24	3.44	4.27	3.82	3.13
K_2O	1.06	1.69	1.45	1.84	2.05	1.32	2.21	2.23	1.97	1.47	1.85	2.08	2.55	1.63	1.90	1.41
P_2O_5	0.51	1.06	0.64	0.75	0.76	1.34	0.82	0.96	0.85	0.91	0.95	0.99	1.12	1.13	1.25	0.85
LOI	0.96	3.85	5.12	5.24	4.65	4.77	5.02	4.96	3.83	4.08	4.29	4.45	2.56	4.12	4.59	3.85
Trace Elements, ppm																
Sc	22	15	20	15	19	21	12	11	16	19	12	9	13	13	13	20
V	217	164	251	212	212	243	164	99	219	199	152	127	150	148	144	245
Cr	241	94	85	7	54	7	10	74	19	103	7	5	19	20	4	102
Co	50	41	46	33	43	37	36	31	47	46	33	29	37	36	34	50
Ni	160	95	66	12	65	18	36	69	55	116	28	20	36	35	17	90
Cu	63	51	55	38	58	47	45	35	65	58	56	41	52	50	45	70
Rb	26.3	51	52	84	63	67	83	77	62	53	54	65	129	59	55	62
Sr	620	909	807	845	817	903	1031	1084	933	772	962	927	882	905	1214	650
Y	28.0	36	34	27.9	36	29.8	31.3	34	32	32	34	31	38	38	36	33
Zr	198	438	271	247	311	184	396	460	351	333	467	507	445	465	277	297
Nb	54	83	56	60	69	47	77	91	73	65	90	94	77	81	59	64
Mo	3.2	4.9	2.8	2.0	3.6	1.4	5.1	5.0	3.8	3.5	3.4	4.6	4.0	4.7	2.8	2.0
Cs	0.39	2.28	11.4	7.7	5.0	8.2	7.7	4.9	2.73	3.9	1.04	1.74	9.8	5.0	7.6	1.61
Ba	305	667	364	320	408	429	596	563	527	404	679	552	458	466	369	347
La	38	67	41	41	49	39	60	71	55	52	70	74	61	64	47	46
Ce	75	137	89	87	103	82	123	143	116	107	141	146	129	132	105	93
Pr	9.5	16.8	11.3	10.8	12.7	10.6	14.8	16.5	15.1	14.4	17.1	17.3	16.1	16.4	13.7	11.9
Nd	37	66	47	43	52	46	60	67	59	54	66	67	66	66	59	49
Sm	7.5	12.6	9.8	8.7	10.6	9.7	11.5	12.6	12.0	10.7	12.7	12.3	12.9	12.8	12.0	10.6
Eu	2.34	3.7	3.1	2.79	3.3	3.7	3.7	3.9	3.6	3.3	3.8	3.6	4.0	4.1	4.0	3.4
Gd	6.6	10.3	8.2	7.3	8.9	8.3	9.2	9.6	9.6	9.0	10.2	9.3	10.7	10.6	10.0	9.5
Tb	1.02	1.54	1.26	1.10	1.31	1.18	1.34	1.39	1.40	1.35	1.49	1.36	1.60	1.61	1.44	1.41
Dy	5.6	7.7	6.6	5.5	6.9	5.9	6.5	7.0	7.0	6.8	7.4	6.6	8.1	7.9	7.4	7.3
Ho	1.07	1.36	1.19	1.00	1.25	1.06	1.11	1.18	1.20	1.24	1.31	1.18	1.42	1.41	1.30	1.23
Er	2.44	3.2	2.95	2.36	3.1	2.54	2.59	2.76	2.53	2.73	2.77	2.40	3.2	3.3	3.3	2.92
Tm	0.35	0.42	0.40	0.32	0.42	0.32	0.32	0.36	0.33	0.35	0.36	0.28	0.42	0.44	0.41	0.38
Yb	2.14	2.19	2.27	1.75	2.38	1.83	1.81	1.89	1.91	2.17	2.14	1.64	2.34	2.37	2.53	2.02
Lu	0.28	0.32	0.32	0.26	0.36	0.27	0.26	0.27	0.23	0.27	0.25	0.22	0.33	0.34	0.36	0.29
Hf	4.8	10.1	6.5	4.2	6.8	4.5	9.1	9.7	8.6	7.6	9.8		9.4	10.3	5.5	7.3
Ta	3.4	5.5	3.5	3.8	4.3	3.1	4.9	5.8	4.7	4.2	6.0	6.5	5.1	5.5	3.6	4.4
Pb	2.2	5.0	7.1		9.1	7.2	8.7	8.8	4.6	4.1	7.6	6.5	7.0	8.0	4.0	2.9
Th	4.5	7.9	4.1	4.2	5.3	3.4	7.6	9.5	5.9	5.4	8.5	8.3	6.0	7.0	4.4	4.6
U	1.35	2.38	1.22	1.18	1.77	1.07	4.3	3.3	2.12	1.85	2.60	2.33	1.73	2.10	1.27	1.48

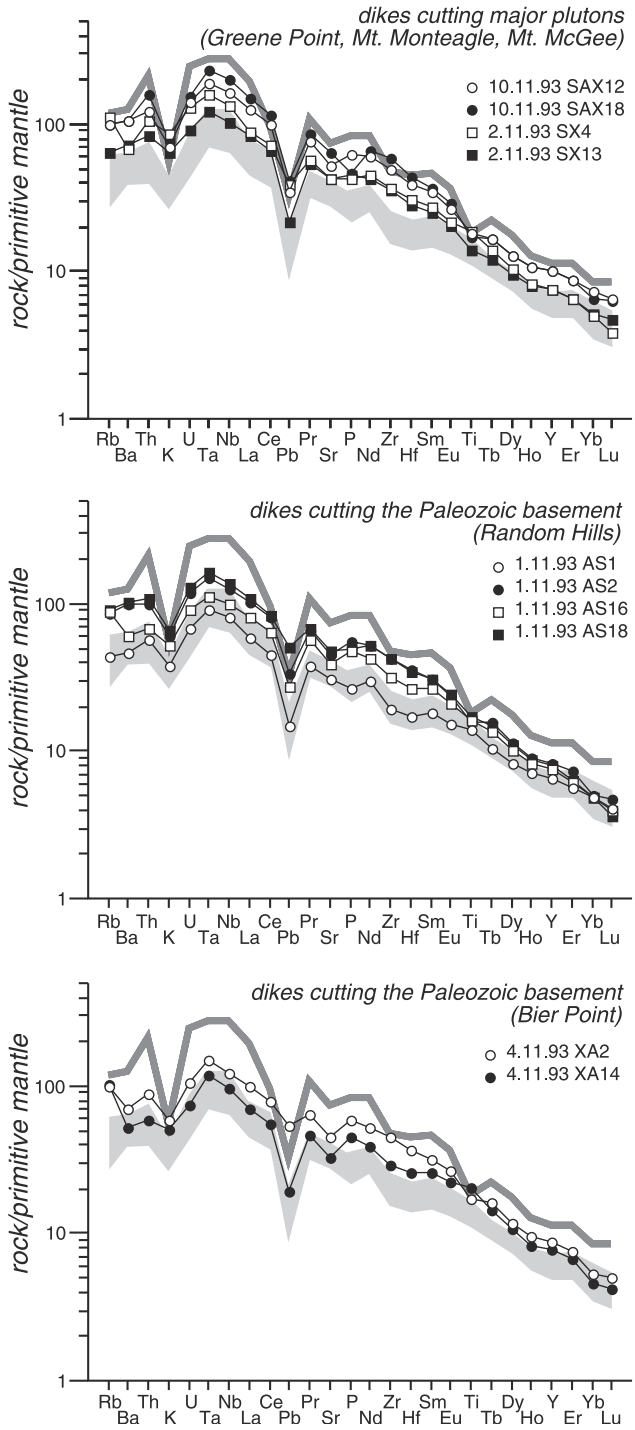

Figure 7. Primitive mantle normalized multielement spidergrams of selected mafic dike samples. Normalizing values after *McDonough and Sun* [1995]. MMVG-NVL, Neogene primitive lavas from northern Victoria Land (unpublished data from the authors).

[1997], based on the same assumptions as above. The enrichment ratios obtained show that the partitioning of K between the source and the melt is characterized by lower enrichment with respect to elements, such as U, Nb, Ta, La, and Ce, that have very similar degrees of incompatibility during the melting of lherzolite containing only anhydrous phases.

[24] When the same type of modeling is performed using a selection from the Neogene primitive lavas from NVL (unpublished data from the authors), the spidergram of the obtained source (Figure 10) is indistinguishable, within the statistical error, from that obtained for dikes. Also for lavas the bulk partition coefficients and enrichment ratios show the same distribution as for dikes, arguing for the occurrence of a residual potassic phase, either amphibole or phlogopite, as suggested by the melting experiments of *Orlando et al.* [2000]. Even if the nature of such a potassic phase is difficult to constrain [*Class and Goldstein*, 1997], the most significant issue is that a hydrous phase is present in the source in both cases.

[25] These chemical features can be described in terms of mantle components on the basis of incompatible element ratios [*Weaver*, 1991] and isotopic compositions [*Zindler and Hart*, 1986; *Hofmann*, 1997]. Based on this type of taxonomy, *Hart and Kyle* [1993] reported evidence for a HIMU (high $^{238}U/^{204}Pb$) component in the source of McMurdo Volcanic Group products. On the other hand, *Rocholl et al.* [1995] described the source of Neogene lavas of NVL as a space-time-variable combination of EM1 (enriched mantle-type 1), HIMU and DMM (depleted mantle source of mid-ocean ridge basalts, MORB) components residing in progressively deeper stratified mantle. *Hart et al.* [1997] found that a prevalent mixing end-member in the source of volcanic rocks from the Hobbs Coast of Marie Byrd Land and the whole WARS volcanism is represented by the FOZO mantle component (focal zone of convergence of isotopic arrays for ocean island basalts [*Hart et al.*, 1992; *Hofmann*, 1997]). Additionally, high $^{206}Pb/^{204}Pb$ for Coleman Nunatak and Crary Mountains lavas are interpreted as evidence for HIMU component in their source [*Hart et al.*, 1997; *Panter et al.*, 2000]. The source of NVL Eocene dikes shows incompatible element ratios suggestive of a HIMU component [*Weaver*, 1991]. On the other hand, Sr-Nd isotopes are akin to the C (common) mantle component (point of convergence of isotope arrays for MORB [*Hanan and Graham*, 1996]). Even if a conclusive statement requires also Pb isotopes data, it is worth noting that Pb isotope compositions of NVL Neogene lavas [*Rocholl et al.*, 1995] cluster on C compositions, with a very modest shift toward HIMU. However, the mantle components are probably small or mesoscale features rather than physically separated reservoirs [*Chauvel et al.*, 1992; *Halliday et al.*, 1995; *Dostal et al.*, 1998; *Saal et al.*, 1998].

[26] Therefore we retain as first-order evidence that the source of NVL magmas is a typical OIB-like source containing a residual hydrous potassic phase. Additionally, the geochemical and isotopic diversity within the Western Ross Supergroup in NVL is small relative to the duration ($\approx$ 50 m.y.) and areal extent (200 $\times$ 80 km) of magmatic activity.

5.2. Chronological Relations Between Magmatism and Tectonics

[27] Magmatic activity started in NVL at middle Eocene with emplacement of bimodal intrusions and mafic dike swarms in the Campbell-Icebreaker Glaciers area (Figures 3 and 5). The internally isotropic plutons are weakly elon-

Table 5. Rb-Sr and Sm-Nd Isotopic Data of Cenozoic Plutons and Dikes From Northern Victoria Land[a]

Sample	Age, Ma	Notes	Rb, ppm	Sr, ppm	$^{87}Sr/^{86}Sr$ Measured ± 2σ	$^{87}Rb/^{86}Sr$	$^{87}Sr/^{86}Sr$ t	$^{143}Nd/^{144}Nd$ Measured ± 2σ	$^{147}Sm/^{144}Nd$	$^{143}Nd/^{144}Nd$ *t*	e_{Nd} *t*
Greene Point Igneous Complex											
21-10-93 A1c	47.5	1, 3, 4	8.6	1414	0.703637 ± 8	0.018	0.70363	0.512854 ± 11	0.1200	0.512817	4.7
21-10-93 A1d	39.2	1, 3, 4	17.3	1239	0.703516 ± 10	0.040	0.70349	0.512874 ± 7	0.1219	0.512843	5.0
21-10-93 A1e	42.7	1, 3, 4	54.1	1091	0.703523 ± 9	0.143	0.70344	0.512850 ± 15	0.1110	0.512819	4.6
21-10-93 A1a	38.6	1, 3, 4	157.4	183	0.705086 ± 12	2.488	0.70372	0.512839 ± 12	0.1367	0.512804	4.2
10-11-93 SAX7	*40.0*	1, 4, 5	90	9.37	0.71997 ± 3	27.77	0.70419	0.512814 ± 8	0.0808	0.512793	4.0
10-11-93 SAX17	*40.0*	1, 5	93	7.64	0.72637 ± 3	35.40	0.70626	0.512827 ± 8	0.1342	0.512792	4.0
10.11.93 SAX22	*40.0*	1, 3,	*4.9*	*1258*	0.703610 ± 10	0.011	0.70360	0.512850 ± 9	0.1203	0.512819	4.5
10-11-93 SAX1a	39.2	2, 3, 4	93.8	1028	0.703542 ± 8	0.264	0.70340	0.512866 ± 13	0.1211	0.512835	4.8
10.11.93 SAX2	39.2	2, 4, 5	121	21	0.71346 ± 3	16.36	0.70435	0.512848 ± 7	0.1150	0.51819	4.5
10-11-93 SAX8	39.7	2, 3, 4	49.6	922	0.703714 ± 10	0.156	0.70363	0.512851 ± 10	0.1195	0.512820	4.5
10.11.93 SAX12	*30.0*	2, 3	*60*	*1049*	0.703624 ± 16	0.166	0.70355	0.512860 ± 9	0.1131	0.512838	4.7
10.11.93 SAX18	*30.0*	2, 4	58.2	1405	0.703280 ± 11	0.120	0.70323	0.512843 ± 5	0.1077	0.512822	4.4
10.11.93 SAX19	*30.0*	2, 4	55.7	1021	0.703686 ± 11	0.158	0.70362	0.512846 ± 7	0.1160	0.512823	4.4
Mt. Monteagle Igneous Complex											
2.11.93 SX1a	*42.5*	1, 5	154	12.4	0.73482 ± 3	36.19	0.71297	0.512864 ± 12	0.1009	0.512836	5.0
2.11.93 SX10[b]	*42.5*	1, 3, 4	23.4	758	0.704284 ± 14	0.089	0.70423	0.512777 ± 8	0.1329	0.512740	3.1
28.1.91 LZ53	42.5	2, 4, 5	72.8	972	0.70364 ± 2	0.217	0.70351	0.512856 ± 9	0.1021	0.512828	4.8
2.11.93 SX4	*42.5*	2, 3	*67*	*843*	0.703404 ± 11	0.231	0.70326	0.512893 ± 8	0.1222	0.512859	5.4
2.11.93 SX9	*42.5*	2, 3	*57*	*670*	0.703609 ± 11	0.246	0.70346	0.512867 ± 10	0.1208	0.512833	4.9
Mt. McGee Igneous Complex											
19.1.91 LZ 42	38.1	1, 4, 5	35	1298	0.70507 ± 2	0.078	0.70503	0.512720 ± 7	0.1181	0.512691	2.0
02.11.93 SX12	38.0	1, 4	77.4	565	0.704625 ± 10	0.396	0.70441	0.512774 ± 10	0.1110	0.512746	3.1
21.11.93 SX3	38.0	1, 4	38.6	250	0.705030 ± 10	0.446	0.70479	0.512759 ± 6	0.1209	0.512729	2.7
2.11.93 SX13	*30.0*	2, 3	*38.8*	*840*	0.703330 ± 11	0.134	0.70327	0.512910 ± 10	0.1155	0.512887	5.7
2.11.93 SX17	*30.0*	2, 3	*42.9*	*736*	0.703728 ± 11	0.169	0.70366	0.512865 ± *9*	0.1292	0.512840	4.8
2.11.93 SX18	*30.0*	2, 3	*44.4*	*706*	0.703817 ± 13	0.182	0.70374	0.512867 ± 7	0.1263	0.512842	4.8
Random Hills Dike Swarm											
1.11.93 AS1	*40.0*	2, 3	26.3	620	0.703057 ± 10	0.123	0.70299	0.512941 ± 12	0.1226	0.512909	6.3
1.11.93 AS2	*40.0*	2, 3	51.0	909	0.703598 ± 12	0.162	0.70351	0.512907 ± 10	0.1154	0.512877	5.7
1.11.93 AS18	*40.0*	2, 3	54.0	962	0.703570 ± 12	0.162	0.70348	0.512900 ± 11	0.1163	0.512870	5.5
Bier Point Dike Swarm											
4.11.93 XA14	*45.0*	2, 3	62.0	650	0.703831 ± 10	0.276	0.70365	0.512895 ± 10	0.1308	0.512857	5.4

[a] Ages in italics are assumed based on geological relationships with dated rocks. Rb and Sr concentration in italics are determined by ICP-MS, the remainder by ID; $^{147}Sm/^{144}Nd$ calculated from Sm and Nd ICP-MS determination (Tables 3 and 4).

[b] Notes are 1, plutonic rock; 2, dike sample; 3, $^{87}Sr/^{86}Sr$ determination on leached whole rock powder; 4, Rb-Sr data from *Tonarini et al.* [1997]; 5, Sr isotope data determined by VG54E TIMS, the remainder are determined by Finnigan MAT262 TIMS.

gated parallel to and located on the main Cenozoic transfer fault systems [*Salvini et al.*, 1997; *Ferraccioli and Bozzo*, 1999], inherited from the NW-SE to NNW-SSE deep-reaching tectonic discontinuities that formed during the early Paleozoic Ross Orogeny and linked to the oceanic fracture zones between Australia and Antarctica [*Foster and Gleadow*, 1992]. The overall strikes of the dikes (Figures 2 and 3) are either parallel to or at about 40° to the main fault trends. We infer that the plutons were emplaced during and/or after the activity of the main faults, as magma pooled in pull-apart "voids" generated by the activity of the strike-slip-transtensional faults. The dikes are mostly coeval with the plutons (Figure 5a), and their bimodal strike distribution is fully compatible with emplacement related to the same tectonic episode: NW-SE dikes were emplaced on the main transtensional faults, while N-S dikes were emplaced at the same time (Figure 5c) on the tensional-transtensional faults that developed between the main faults as a kinematic consequence of dextral transcurrence [*Salvini and Storti*, 1999; *Storti et al.*, 2001]. Also, in the adjoining area of southern Victoria Land, emplacement of widespread Cenozoic dikes is controlled by right-lateral transtensional tectonics [*Rossetti et al.*, 2000]. First-order evidence is then that the ascent and emplacement of magmas is chronologically, geographically and structurally-linked to the activity of the main Cenozoic fault systems.

[28] The onset of magmatism and intracontinental deformation in NVL is coeval with a global Eocene plate reorganization, when the spreading rate between Australia and Antarctica started to increase [*Cande and Mutter*, 1982; *Lawver et al.*, 1991; *Lithgow-Bertelloni and Richards*, 1998; *Veevers*, 2000]. Moreover, the change from Cretaceous extension to Eocene transtension could have helped to accommodate significant movement in the Southern Ocean with limited extension in the Ross Sea area during the Cenozoic.

[29] During late Oligocene, magmatism was active in the area between Icebreaker and Borchgrevink Glaciers (Figures 3 and 5d). The different timing in the magmatic activity of the fault-bounded Campbell-Icebreaker area (middle Eocene to Oligocene) and the Icebreaker-Borchgrevink area (Oligocene to late Miocene) lends further support to a close relationship between magmatism and regional tectonics.

[30] During Miocene, volcanic activity in the Ross Embayment began to affect southern Victoria Land and

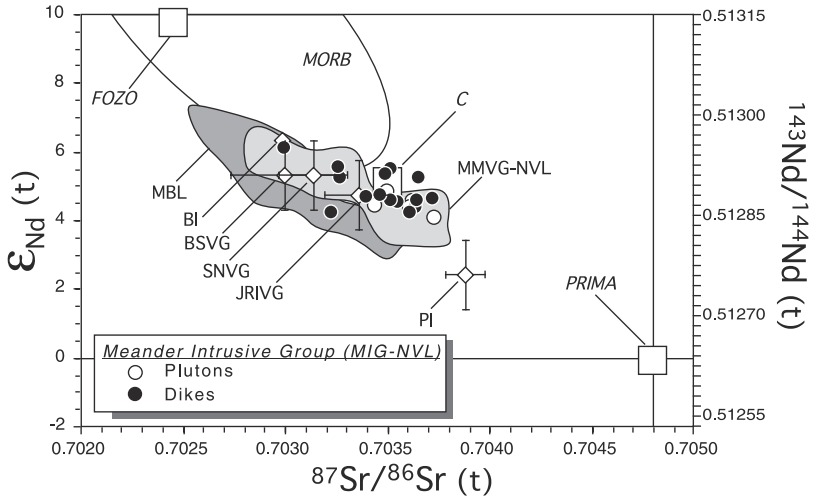

Figure 8. The ratio $\varepsilon_{Nd}(t)$ versus $^{87}Sr/^{86}Sr(t)$ calculated at the time of emplacement for plutons and dikes from northern Victoria Land between Campbell and Icebreaker Glaciers. Also shown are: fields for Neogene lavas from northern Victoria Land (MMVG-NVL) and Marie Byrd Land (MBL); average values (with 1 SD) for Cenozoic volcanic provinces of the Antarctic Plate; mid-ocean ridge basalts (MORB) field; mantle components discussed in the text. Sources of data are as follows: MMVG-NVL, *Wörner et al.* [1989], *Rocholl et al.* [1995], and unpublished data from the authors; MBL, *Hole and LeMasurier* [1994], *Hart et al.* [1997], and *Panter et al.* [2000]; Peter I Øy (PI), *Prestvik et al.* [1990] and *Hart et al.* [1995]; Balleny Islands (BI), *Hart* [1988]; James Ross Island Volcanic Group (JRIVG, Antarctic Peninsula), *Hole et al.* [1995] and *Lawver et al.* [1995]; Seal Nunataks Volcanic Group (SNVG, Antarctic Peninsula), *Hole* [1990] and *Hole et al.* [1993]; Bellingshausen Sea Volcanic Group (BSVG, Alexander Island, Antarctic Peninsula), *Hole* [1988] and *Hole et al.* [1993]; MORB, primitive mantle (PRIMA), focal zone mantle component (FOZO), and C mantle component after *Hofmann* [1997].

northern Victoria Land north of Campbell Glacier. A 200 km gap existed between the two volcanically active areas. The gap could be reduced to 100 km if the submarine volcanoes within the Terror Rift inferred from magnetic anomalies [*LeMasurier and Thomson*, 1990] would have Miocene age. The distribution of volcanic activity in crustal sectors separated by a >100 gap, together with the location of the whole Erebus Volcanic Province along transverse structures within the Discovery accommodation zone [*Wilson*, 1999], are additional evidence for tectonic controls on magmatism.

6. Critical Review of Plume Models for WARS Magmatism

6.1. Comparison of NVL Magma Source With Coeval Neighboring Sources

[31] The geochemical features of plutons, dikes and lavas from NVL are common to the whole Western Ross Supergroup. In fact, the most mafic products from the active Mt. Erebus volcano of southern Victoria Land display trace element distributions (Figure 11a) and Sr isotope ratios equivalent to NVL dikes and lavas [*Kyle et al.*, 1992]. Also the mafic lavas from the other important volcanic province on the opposite side of the WARS in a quite different crustal tectonic framework (Marie Byrd Land) have geochemical features very similar to NVL dikes and lavas, as already pointed out by *Hole and LeMasurier* [1994] on the basis of Sr-Nd isotope data. The modeled source to Hobbs Coast

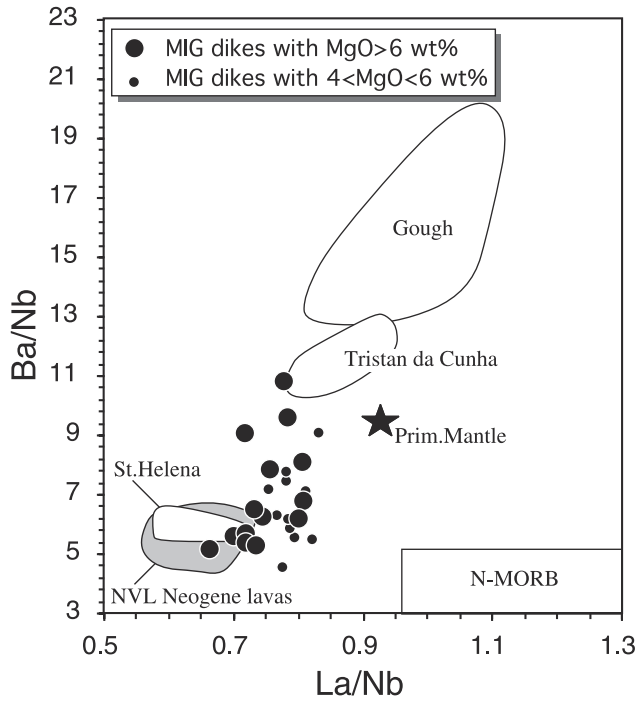

Figure 9. Ba/Nb versus La/Nb diagram. Note that the distribution of data points for dike samples does not change when a different threshold is selected. Reference for primitive mantle, N-MORB, St. Helena, Tristan da Cunha, and Gough values is *Sun and McDonough* [1989].

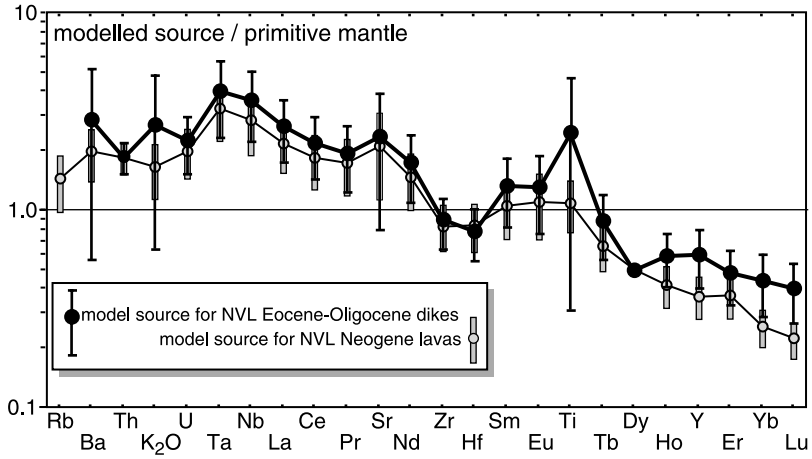

Figure 10. Primitive mantle normalized multielement spidergram for the modeled source to the Eocene-Oligocene mafic dikes and to the Neogene primitive lavas from northern Victoria Land. The modeling approach is the same as *Hart et al.* [1997], with the following assumptions: (1) the incompatible elements ratios in the selected samples only depend on the source composition and melting process, (2) the magma source is unique, and (3) the magma was generated by a modal batch melting process. Normalizing values are after *McDonough and Sun* [1995].

mafic lavas [*Hart et al.*, 1997] displays a distribution of incompatible elements matching that modeled for NVL (Figure 10), as can be predicted from the striking similarity of Primitive Mantle-normalized incompatible element spidergrams of average Marie Byrd Land lavas and NVL Eocene dikes and Neogene lavas (Figures 11a and 12). In addition, the Sr-Nd-Pb isotope data for Western Ross Supergroup and Marie Byrd Land have matching distribution (Figures 8 and 12), halfway between the widespread FOZO and C components [*Hart et al.*, 1997; *Hofmann*, 1997; *Panter et al.*, 2000].

[32] These geochemical features are shared also by Cenozoic volcanic provinces dispersed on the Antarctic plate in areas adjoining the WARS. The volcanic Balleny Islands are located offshore NVL (Figure 1) at the termination of the Balleny Fracture zone against the base of the continental rise, hence at the boundary between continental and oceanic lithosphere. The Balleny Islands basalts display geochemical and isotopic features indistinguishable from those of NVL dikes (Figures 8, 11a, and 12). Peter I Øy is a Pleistocene volcanic island on the opposite side of WARS, offshore Ellsworth Land (Figure 1). It lies on the ocean floor close to the continental rise and adjacent to the formerly active Tharp oceanic fracture zone. The basaltic products [*Hart et al.*, 1995] are again compositionally very similar to NVL dikes and lavas (Figures 8, 11a, and 12).

[33] Another conspicuous Cenozoic volcanic province on the Antarctic plate is located on the Antarctic Peninsula. The overall geochemical features of the Bellingshausen Sea, Seal Nunataks, and James Ross Island volcanic groups are very similar to those of WARS volcanic products (Figures 8, 11b, and 12). They only differ for the relative concentration of most incompatible elements, notably a higher K/Ba ratio [*Hole and LeMasurier*, 1994], associated with the lack of a negative K anomaly in primitive mantle-normalized spidergrams (K/K* in Figure 12). On the other hand, the three provinces of the Antarctic Peninsula differ among each other in negative Ba anomaly (Ba/Ba* in Figure 12). This K-Ba interplay can be explained by invoking the differential K and Ba partitioning between liquid and phlogopite or amphibole [*Halliday et al.*, 1995; *Class and Goldstein*, 1997]. *Hole and LeMasurier* [1994] stated that these features are not affected by increasing melting degree (i.e., they are constant at variable Nb/Y and La/Yb). However, even small degrees of melting could exhaust one or both of the possible potassic phases in the source. Notwithstanding the strongly different geological framework, the difference between Antarctic Peninsula and WARS mostly consists in the role of a possible potassic phase in the source, whereas the remainder of incompatible element distribution and Sr-Nd isotope features are almost indistinguishable (Figures 8, 11b, and 12). Also, in southern Patagonia, close to the boundary between the Antarctic and South American plates (Pali Aike Volcanic Field, $\sim$52°S), Cenozoic basaltic magmas occur with very similar trace element and isotopic compositions (Figures 11b and 12) [*D'Orazio et al.*, 2000]. In both Antarctic Peninsula and southernmost Patagonia, there is agreement on generation of magmas by subslab asthenosphere decompressional melting triggered by the opening of slab-windows or slab roll-back following the cessation of subduction [*Hole et al.*, 1995; *D'Orazio et al.*, 2000]. Therefore similar mantle sources have been active over a wide area in response to very different geological processes, such as continental rifting and slab-window opening.

[34] The geochemical variations of the Cenozoic igneous provinces of the Antarctic Plate appear modest when confronted with both their wide areal distribution and the variation of magmatic setting, continental for NVL-southern Victoria Land-Marie Byrd Land versus oceanic for Balleny Islands-Peter I Øy. Similar isotope and trace element distribution have been observed in volcanic provinces of the Antarctic and South American Plate where melting of the asthenosphere in a slab window setting is acknowledged as the main magma-generating process.

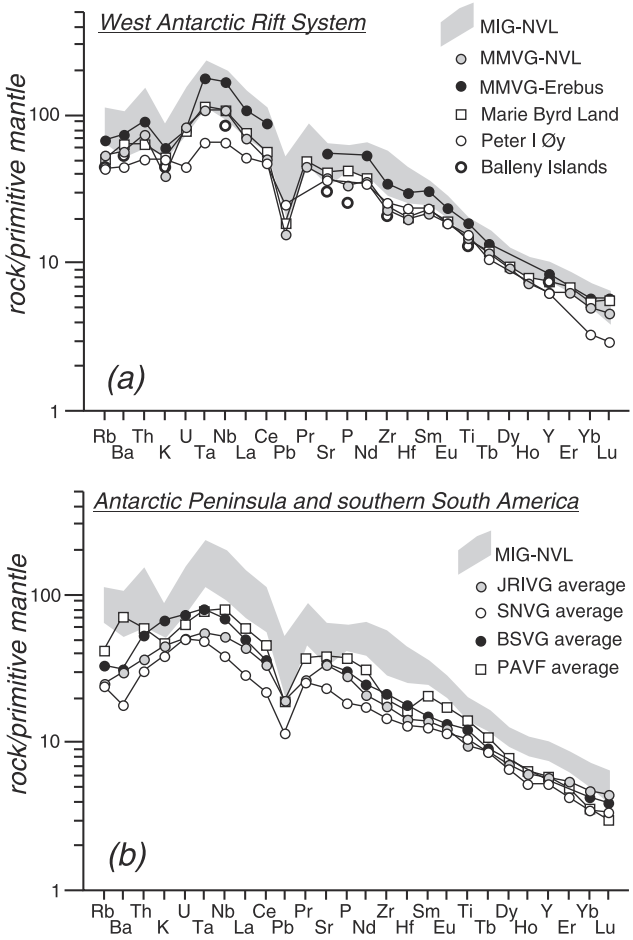

Figure 11. Primitive mantle normalized [*McDonough and Sun*, 1995] multielement spidergrams of averages of (a) volcanic provinces linked to the WARS and (b) volcanic provinces from areas adjoining the WARS. Shaded field represent the variability of the Eocene-Oligocene dikes from northern Victoria Land (MIG-NVL, this work). Averages are calculated from mafic rocks with MgO > 5 wt %. For source of data and abbreviations, see Figure 8 caption plus Erebus volcanic Province (MMVG-EVP), *Kyle et al.* [1992]; Balleny Islands, *Green* [1992]; Pali Aike Volcanic Field (PAVF, southern Patagonia), *D'Orazio et al.* [2000].

[35] The case of Cenozoic magmatism in the Antarctic plate is similar to the Cameroon Line in that evidence is lacking for migration of volcanism with time. This is coupled with first-order homogeneity in geochemical and isotopic features through time and across the ocean-continent boundary [*Fitton and Dunlop*, 1985]. Thus, despite second-order spatial variations leading to refined models [*Halliday et al.*, 1988, 1990], both provinces are large-scale examples of long-lived OIB-like magmatism characterized by chemistry and geographical distribution that are insensitive to time and variation in setting from continental to oceanic.

6.2. Plume or Not Plume?

[36] A basic question about the genetic mechanism of the major continental rifts, as well as for the West Antarctic Rift System, is the conflicting role of active, deep mantle plumes and plate-driven tectonics in ruling magma genesis. A Cenozoic plume beneath the WARS has been postulated originally by *Behrendt et al.* [1991]. This hypothesis is based on (1) the geochemical similarity between the OIB-like basalts from WARS and localities associated with long-lived hot spot tracks [*Hole and LeMasurier*, 1994], (2) the presence in Marie Byrd Land of horst-graben sub-ice topography outlining a large uplifted dome [*LeMasurier and Landis*, 1996], whose growth is associated with both basaltic and felsic volcanism [*LeMasurier and Rex*, 1989], (3) the modest Cenozoic extension in the WARS, suggesting that a mechanism of passive rifting seems at first unable to give way to magmatism, (4) the lack of concurrent plate tectonic mechanisms to produce rifting and volcanism in West Antarctica [*Hole and LeMasurier*, 1994], and (5) the high heat flow of 66–114 mW m^{-2} in the Ross Sea area [*Blackman et al.*, 1987; *Della Vedova et al.*, 1992], coupled with shear wave seismic evidence for anomalously warm upper mantle beneath the Terror Rift and Transantarctic Mountains front [*Bannister et al.*, 2000]. The plume activity has been related either to a single plume centered below Marie Byrd Land [*LeMasurier and Rex*, 1989; *Kyle et al.*, 1991] or to a pair of plumes below Marie Byrd Land and Mt. Erebus, respectively [*Storey et al.*, 1999].

[37] Some of these points are questioned by data from NVL and elsewhere. The activity of a plume with higher-than-normal mantle potential temperature is difficult to reconcile with the prolonged subsidence with basin formation in the Ross Sea during Cretaceous and Cenozoic time. Moreover, in contrast to Marie Byrd Land, NVL is characterized by an elevated linear rift shoulder (the Transantarctic Mountains) dissected by transverse fault systems [*Salvini et al.*, 1997; *Salvini and Storti*, 1999; *Wilson*, 1999] and has no evidence of doming structures. The uplift of the rift shoulder is a long-lasting episodic process that started in early Cretaceous [*Stump and Fitzgerald*, 1992; *Fitzgerald and Stump*, 1997]. Uplift could have been thermally driven [*Smith and Drewry*, 1984; *Berg et al.*, 1989; *Stern and Ten Brink*, 1989], but alternative mechanisms have been proposed such as isostatic uplift of the hanging wall of a major fault cutting the lithosphere [*Stern et al.*, 1992] or uplift linked to a shallow detachment fault in a passive rift setting [*Fitzgerald et al.*, 1986; *Fitzgerald and Baldwin*, 1997].

[38] Besides the uplift issue, the amount of Cenozoic extension is worthy of reconsideration, in light of the larger than previously reported values suggested by *Cande et al.* [2000]. Additionally, in NVL the inception of magmatism is strikingly coeval with a plate tectonic mechanism able to produce rifting and volcanism, namely the middle Eocene global plate reorganization [*Lawver et al.*, 1991; *Lithgow-Bertelloni and Richards*, 1998; *Veevers*, 2000], with increase of spreading rate between Australia and Antarctica [*Cande and Mutter*, 1982; *Richards and Lithgow-Bertelloni*, 1996]. Another problem with the plume model is the unusually low volume of magmatism, even if this could be related to the peculiar setting of the Antarctic plate, stationary and almost completely encircled by mid-ocean ridges [*Hole and LeMasurier*, 1994]. Nevertheless, even the highest volumetric estimates based on geophysical data (>10^6 km^3 [*Behrendt et al.*, 1994, 1996]), when averaged

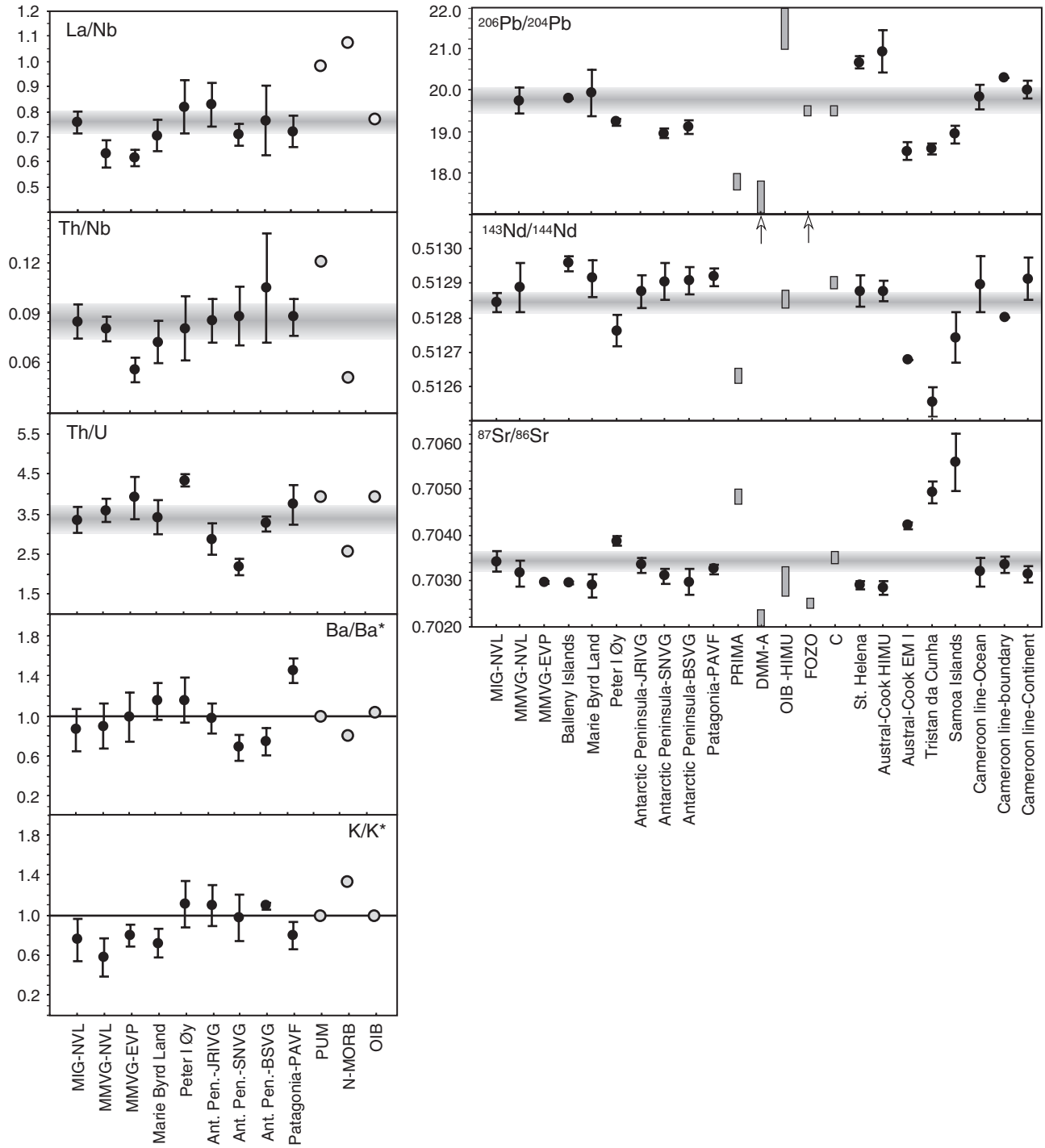

Figure 12. Multiple plot summarizing the geochemical and isotopic variations of mafic igneous rocks across the West Antarctic Rift System, the adjoining, contemporaneously active volcanic provinces, the main mantle components, and basalts commonly used as reference for intraplate magmatism. Ba/Ba* and K/K* are the ratios between the element concentration in the sample and the concentration value interpolated between neighbors in the multielement diagrams of Figure 11. For source of data and abbreviations, see Figure 8 and 11 captions plus St. Helena, Austral-Cook Islands, Tristan da Cunha, Samoa Islands, and Cameroon Line from GEOROC database (available at http://georoc.mpch-mainz.gwdg.de). Trace element values for primitive undifferentiated mantle (PUM), normal mid-ocean ridge basalts (N-MORB), and ocean island basalts (OIB) after *Sun and McDonough* [1989]. Isotope ratios for primitive mantle (PRIMA), depleted MORB mantle-type A (DMM-A), ocean island basalts with high $^{238}U/^{204}Pb$ ratio (OIB-HIMU), focal zone mantle component (FOZO), and C mantle component after *Zindler and Hart* [1986] and *Hofmann* [1997].

over 45–50 Ma provide magma production rates much lower than those expected for melt productivity in a mantle plume-dominated scenario [*Finn et al.*, 2001].

[39] Finally, it is worth noting that slow (hot) mantle in the WARS imaged from surface wave tomography cannot be modelled below 180–200 km [*Danesi and Morelli*, 2000], resulting not deep enough to support plume occurrence. Moreover, the velocity minima are arranged on a line corresponding to the belt of transformation of the Australia-Antarctica ridge [*Danesi and Morelli*, 2000], rather than having the circular symmetry expected for a plume.

[40] The residual support for an active plume(s) hypothesis is then the geochemical similarity of WARS magmas with typical plume-related OIB magmatism. However, the geochemical issue is also fraught with ambiguity. First, the geochemical features of NVL magmatism are common to different settings throughout the Antarctic plate (Figures 8, 11, and 12), and are also indistinguishable from those of Cameroon Line magmatism, which is not associated with a hot spot track (Figure 12). Additionally, it has been pointed out that the thermal regime of even the coldest plumes is sufficient to exhaust a volatile-bearing K-phase in the source [*Smith and Lewis*, 1999], although a possible explanation has been proposed which invokes a role for plume-lithosphere interaction [*Class and Goldstein*, 1997; *Class et al.*, 1998]. Finally, mantle domains rich in hydrous phases are sufficient to explain "hot spot-like" basalt geochemistry without a need for anomalously high mantle temperatures [*Bonatti*, 1990].

6.3. Fossil Plume Head Scenario

[41] A role for a fossil instead of active plume has been proposed by *Rocholl et al.* [1995]. They interpreted the temporal geochemical variability of 15 Ma to Recent volcanic rocks from NVL as due to the increasing involvement of progressively deeper sources in a compositionally stratified mantle, where subcontinental lithospheric mantle is underlain by HIMU mantle (originating from a fossil plume head), which in turn overlays depleted asthenospheric mantle. This model assumes a correspondence between geochemical features and mantle layers. If this is accepted, a significant amount of stretching in the uppermost layers is required in order to generate melt in the up risen, formerly deeper layers, but this conflicts with the small amount of Cenozoic extension inferred for the whole Ross Embayment [*Lawver and Gahagan*, 1994]. Additionally, stretching out of deep mantle layers is a questionable process, because materials at these depth and temperature have a mainly ductile rheological behavior and are weakly coupled with the overlying strong lithosphere [*Anderson*, 1995].

[42] Models have been recently proposed to explain the large-scale geochemical uniformity of magmatism across WARS and a wide area in the Southern Hemisphere [*Hart et al.*, 1997; *Panter et al.*, 2000] that calls for a uniform, geochemically enriched source shared by volcanic provinces thousands of kilometers apart. This requirement could be fulfilled by the occurrence of an ad hoc swarm of plumes with constant geochemical signature. However, this appears to be a special pleading, and more detailed models have been developed invoking a common source which was generated before the late Cretaceous Gondwana breakup, when the areas later affected by Cenozoic magmatism were still joined in a single continental block. Such a source would then have been spread out over the southern oceans during the late Cretaceous and Cenozoic continental drifting. *Hart et al.* [1997] proposed a source constituted of a large fossil multicomponent plume head, which would have impacted and underplated the Antarctic lithosphere prior to late Cretaceous. This plume head would have had an incubation period when (auto)metasomatism processes produced low-melting point, enriched zones/veins. Such a source would have been suitable for magmas during Cenozoic extensional events in Victoria Land, Marie Byrd Land, etc. *Panter et al.* [2000] noted that in Marie Byrd Land true HIMU basalts generated by small-degree partial melting are rather uncommon, whereas lower-μ basalts generated by slightly higher degrees of melting are widespread. On this ground, they suggested that a relatively small, HIMU-type, mantle plume impinged before breakup beneath a large preexisting metasomatised layer within the Gondwanan lithosphere. The timing of plume impingement has to account for the evidence for subsidence, instead of buoyant uplift, reported for that area at late Cretaceous by *LeMasurier and Landis* [1996].

7. Toward an Integrated, Topside-Down Tectonic-Magmatic Model

[43] Dissection of the active plume hypotheses shows that they do not satisfactorily explain the whole tectonic-chronologic-geochemical data set. On the other hand, the main role of fossil plumes is one of building an incompatile element-enriched source with wide extent, reminiscent of the perisphere of *Anderson* [1995]. In the discussion about the role of mantle plumes the tectonic historical perspective is often overlooked, although *Anderson et al.* [1992] and *Sheth* [1999] demonstrated the importance of an accurate time scan of regional events such as crustal doming, lithospheric extension, basin sedimentation, and magmatism in addition to hot spot tracks. We propose that a historically integrated analysis of magmatism and geodynamics of northern Victoria Land and its adjoining areas may offer a wider perspective of WARS activity leading to an alternative and rather simple model for magmatic activity.

[44] The Cenozoic geologic history of NVL provides convincing evidence for space-time link between tectonic and magmatic activity. Therefore the origin of rifting and magmatism has to be explained taking into account combined plate dynamics, regional tectonics and geochemical issues. The geochemical data point out the likely occurrence of a uniform mantle source thousands of km wide below the WARS and adjoining areas of the Antarctic plate and beyond. The historical tectonic-magmatic perspective suggests that the role of mantle plume(s) is not fully constrained, whereas intraplate tectonic displacements induced by plate circuit in the Southern Hemisphere appear sufficient to explain generation and emplacement of magmas.

[45] We propose a model in which the WARS magmatism is top side-down controlled, that is, plate dynamics is able to generate a suitable magma source in late Cretaceous, and local tectonics is able to sample such a source during the Cenozoic. The late Cretaceous drifting of New Zealand

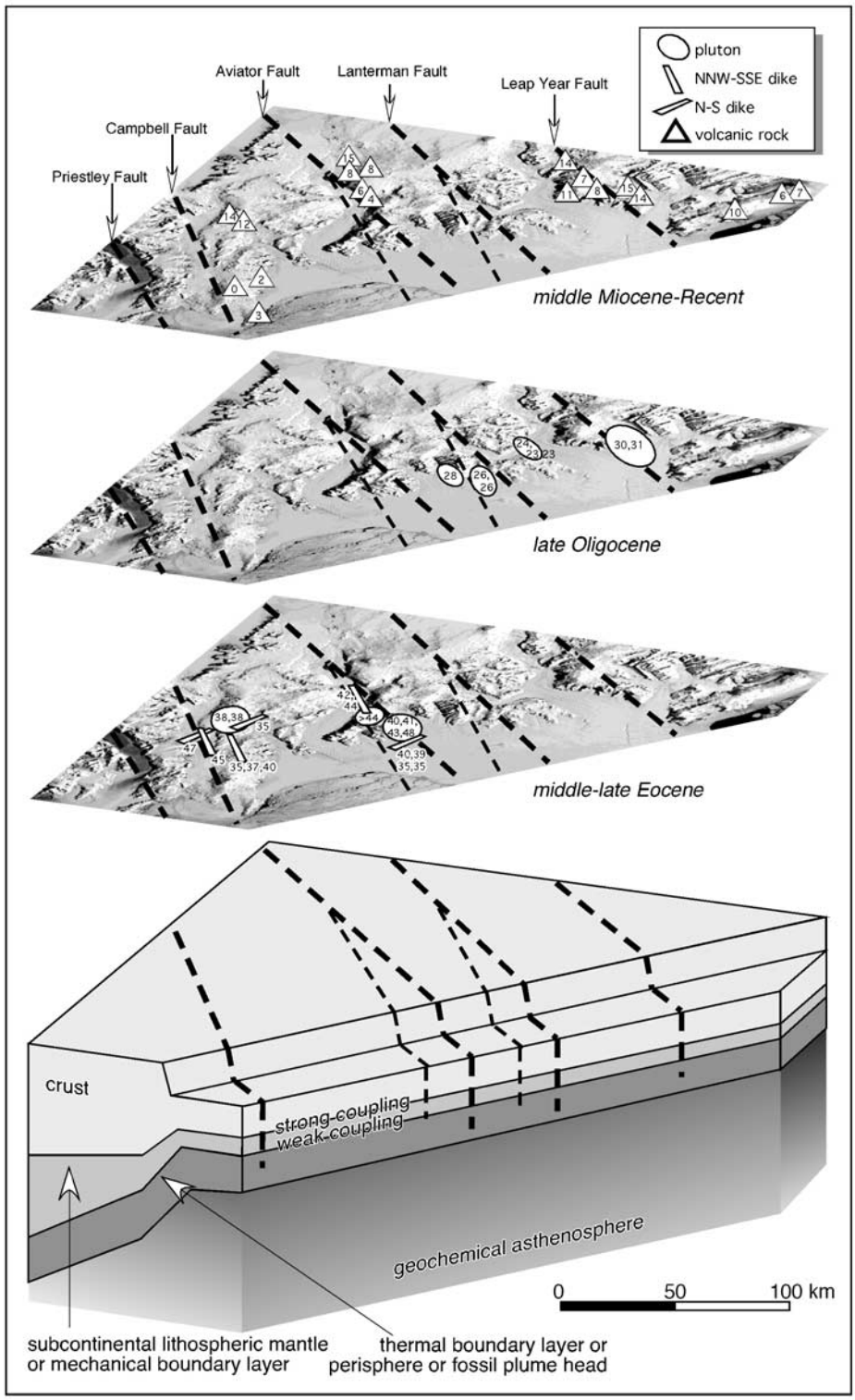

Figure 13. Chronologic-geographic-structural summary for the Cenozoic igneous activity in northern Victoria Land and interpretive cartoon for magma genesis. Base satellite image is an oblique view of the same image of Figure 3b. Numbers inside or besides pluton, dike, and volcanic rock symbols represent isotopic age, taken from *Müller et al.* [1991], *Tonarini et al.* [1997], *Rocchi et al.* [2002], *Armienti and Baroni* [1999], and this work.

continental block away from Antarctica led to crustal stretching and opening of the main sedimentary basins in the Ross Sea. At the same time, stretching affected the strong subcrustal lithosphere, possibly at a even higher rate, as postulated by *Behrendt* [1999] for late Cenozoic times. The underlying weak layer (either the lower part of the thermal boundary layer, or the perisphere [*Anderson*, 1995], or a fossil plume head), was decompressed to its wet/CO_2-rich solidus, and became veined by small degree melts. At around 43 Ma, the increased differential velocity along the Balleny Fracture Zone forced the Southern Oceans fracture zones to extend across NVL as translithospheric dextral strike-slip systems, inducing lithospheric pull-apart and small-scale mantle convection [*Anderson*, 1995] at the edge of East Antarctic Craton. This triggered decompression melting of widespread low-melting point domains in the shallow, weak, enriched layer. In this model (Figure 13), the main fault systems are not only the site of magma rise, rather they are translithospheric discontinuities [*Bailey*, 1983] that, when associated with even a minimal amount of stretching, are capable to trigger decompression melting in the already decompressed, shallow, enriched layer, or at least in its enriched veins/zones. The best permeability conditions for magma ascent occur on deep-penetrating discrete faults in the brittle-volcanic belt, at the transition between the onshore thick brittle domain and the offshore thinner, more ductile region characterized by partitioning of deformation on a great number of small-scale faults [*Salvini et al.*, 1997].

8. Conclusions

[46] The Cenozoic geologic history of NVL is replete with compelling evidence for close space-time link between magmatic activity, dextral strike-slip fault systems, and Southern Ocean fracture zones. In NVL, the source of magmas is nearly uniform throughout 50 m.y. This type of mantle source is thousands of kilometers wide below the WARS and adjoining areas of the Antarctic plate. Moreover, the first-order geochemical and isotopic features of WARS magmatism match those of common OIB-like products from within-plate setting, either from oceanic islands, continental rifts or mixed settings. Timing of magmatism-uplift-extension-rifting in NVL and WARS conflicts with the occurrence of an active mantle plume. On the other hand, intraplate tectonic displacements induced by plate circuit in the Southern Hemisphere appear sufficient to explain both (1) emplacement of magmas tightly linked with active lithospheric structures and (2) episodic melting of a widespread, enriched/veined low-melting point mantle source. A model is proposed in which the Southern Ocean fracture zones extend across northern Victoria Land as translithospheric strike-slip systems, promoting local decompression melting of widespread low-melting point domains in a shallow, weak, enriched layer. This could be a fossil plume head or, as we propose, a layer decompressed to its wet/CO_2-rich solidus and then veined by small degree melts during the late Cretaceous amagmatic rift phase. In conclusion, the role of plume activity in the WARS is not overruled, but alternative hypotheses (that account for historically integrated geochemical-tectonic-plate dynamics data) are worthy of consideration.

[47] **Acknowledgments.** We wish to thank the alpine guides and the helicopter pilots, which helped us in discovering new intrusions and dike swarms and better studying those already known by earlier studies. F. Ferraccioli, W. E. LeMasurier, and F. Storti provided useful suggestion on earlier versions of the manuscript. J. G. Fitton kindly provided a comprehensive major and trace element data set for the Cameroon Line. P. Kyle, L. Lawver, and M. J. Walter provided thorough reviews which greatly helped us to improve the original manuscript. ICP-MS instrument and clean lab facilities were funded by the National Group for Volcanology and the National Program for Research in Antarctica of Italy (PNRA), respectively. The whole work has been financially supported by the PNRA.

References

Anderson, D. L., Lithosphere, asthenosphere, and perisphere, *Rev. Geophys.*, *33*(1), 125–149, 1995.

Anderson, D. L., Y.-S. Zhang, and T. Tanimoto, Plume heads, continental lithosphere, flood basalts and tomography, in *Magmatism and the Causes of Continental Break-up*, edited by B. C. Storey, T. Alabaster, and R. J. Pankhurst, *Geol. Soc. Spec. Publ.*, *68*, 99–124, 1992.

Armienti, P., and C. Baroni, Cenozoic climatic change in Antarctica recorded by volcanic activity and landscape evolution, *Geology*, *27*(7), 617–620, 1999.

Armienti, P., L. Civetta, F. Innocenti, P. Manetti, A. Tripodo, L. Villari, and G. Vita, New petrological and geochemical data on Mt. Melbourne volcanic field, Northern Victoria Land, Antarctica. (II Italian Antarctic Expedition), *Mem. Soc. Geol. It.*, *46*, 397–424, 1991.

Bailey, D. K., The chemical and thermal evolution of rifts, *Tectonophysics*, *94*, 585–597, 1983.

Balestrieri, M. L., G. Bigazzi, C. Ghezzo, and B. Lombardo, Fission track dating of apatites from the Granite Harbour Intrusive suite and uplift-denudation history of the Transantarctic Mountains in the area between David and Mariner Glaciers (Northern Victoria Land, Antarctica), *Terra Antarct.*, *1*(1), 82–87, 1994.

Bannister, S., R. K. Snieder, and M. L. Passier, Shear-wave velocities under the Transantarctic Mountains and Terror Rift from surface wave inversion, *Geophys. Res. Lett.*, *27*, 281–284, 2000.

Behrendt, J. C., Crustal and lithospheric structure of the West Antarctic Rift System from geophysical investigations—A review, *Global Planet. Change*, *23*, 25–44, 1999.

Behrendt, J. C., W. E. LeMasurier, A. K. Cooper, F. Tessensohn, A. Tréhu, and D. Damaske, Geophysical studies of the West Antarctic Rift System, *Tectonics*, *10*(6), 1257–1273, 1991.

Behrendt, J. C., W. LeMasurier, and A. K. Cooper, The West Antarctic Rift System—A propagating rift captured by a mantle plume?, in *Recent Progress in Antarctic Earth Science*, edited by Y. Yoshida, K. Kaminuma, and K. Shiraishi, pp. 315–322, Terra Sci., Tokyo, 1992.

Behrendt, J. C., D. D. Blankenship, C. A. Finn, R. E. Bell, R. E. Sweeney, S. M. Hodge, and J. M. Brozena, CASERTZ aeromagnetic data reveal late Cenozoic flood basalts(?) in the West Antarctic Rift System, *Geology*, *22*, 527–530, 1994.

Behrendt, J. C., R. Saltus, D. Damaske, A. McCafferty, C. A. Finn, D. Blankenship, and R. E. Bell, Patterns of late Cenozoic volcanic and tectonic activity in the West Antarctic Rift System revealed by aeromagnetic surveys, *Tectonics*, *15*(2), 660–676, 1996.

Berg, J. H., R. J. Moscati, and D. L. Herz, A petrologic geotherm from a continental rift in Antarctica, *Earth Planet. Sci. Lett.*, *93*, 98–108, 1989.

Blackman, D. K., R. P. V. Herzen, and L. A. Lawver, Heat flow and tectonics of the western Ross Sea area, Antarctica, in *The Antarctic Continental Margin: Geology and Geophysics of the Western Ross Sea*, *Earth Sci. Ser.*, vol. 5B, edited by A. K. Cooper and F. J. Davey, pp. 179–189, Circum-Pac. Counc. for Energy and Miner. Resour., Houston, Tex., 1987.

Bonatti, E., Not so hot "hot spots" in the oceanic mantle, *Science*, *250*, 107–111, 1990.

Cande, S. C., and J. C. Mutter, A revised identification of the oldest sea-floor spreading anomalies between Australia and Antarctica, *Earth Planet. Sci. Lett.*, *58*, 151–160, 1982.

Cande, S. C., J. M. Stock, R. D. Müller, and T. Ishihara, Cenozoic motion between East and West Antarctica, *Nature*, *404*, 145–150, 2000.

Cape Roberts Science Team, Studies from the Cape Roberts Project: Initial report on CRP-2/2A, Ross Sea, Antarctica—Summary of results, *Terra Antarct.*, *6*, 156–169, 1999.

Chand, S., M. Radhakrishna, and C. Subrahmanyam, India-East Antarctica conjugate margins: Rift-shear tectonic setting inferred from gravity and bathymetry data, *Earth Planet. Sci. Lett.*, *185*, 225–236, 2001.

Chauvel, C., S. R. Hart, and P. Vidal, HIMU-EM: The French Polynesian connection, *Earth Planet. Sci. Lett.*, *110*, 99–119, 1992.

Class, C., and S. L. Goldstein, Plume-lithosphere interactions in the ocean basins: constraints from the source mineralogy, *Earth Planet. Sci. Lett.*, *150*, 245–260, 1997.

Class, C., S. L. Goldstein, R. Altherr, and P. Bachèlery, The process of plume-lithosphere interactions in the ocean basins—The case of Grande Comore, *J. Petrol.*, *39*, 881–903, 1998.

Danesi, S., and A. Morelli, Group velocity of Rayleigh waves in the Antarctic region, *Phys. Earth Planet. Inter.*, *122*, 55–66, 2000.

Della Vedova, B., G. Pellis, L. A. Lawver, and G. Brancolini, Heat flow and tectonics of the western Ross Sea, in *Recent Progress in Antarctic Earth Science*, edited by Y. Yoshida, K. Kaminuma, and K. Shiraishi, pp. 627–637, Terra Sci., Tokyo, 1992.

DiVenere, V. J., D. V. Kent, and I. W. D. Dalziel, Mid-Cretaceous paleomagnetic results from Marie Byrd land, West Antarctica: A test of 100 Ma relative motion between East and West Antarctica, *J. Geophys. Res.*, *99*(B8), 15,115–15,139, 1994.

D'Orazio, M., S. Agostini, F. Mazzarini, F. Innocenti, P. Manetti, M. J. Haller, and A. Lahsen, The Pali Aike Volcanic Field, Patagonia: Slab-window magmatism near the tip of South America, *Tectonophysics*, *321*, 407–427, 2000.

Dostal, J., B. Cousens, and C. Dupuy, The incompatible element characteristics of an ancient subducted sedimentary component in ocean island basalts from French Polynesia, *J. Petrol.*, *39*, 937–952, 1998.

Duffield, W. A., and G. B. Dalrymple, The Taylor Creek Rhyolite of New Mexico: A rapidly emplaced field of lava domes and flows, *Bull. Volcanol.*, *52*, 475–487, 1990.

Elliot, D. H., Paleovolcanological setting of the middle Jurassic Mawson Formation: Evidence from the Prince Albert Mountains, Victoria Land, paper presented at the 8th International Symposium on Antarctic Earth Sciences, Victoria Univ., Wellington, New Zealand, 1999.

Ferraccioli, F., and E. Bozzo, Crustal features inherited from Paleozoic terranes and tectonic blocks of the Transantarctic Mountains: An aeromagnetic perspective, *J. Geophys. Res.*, *104*(B11), 25,297–25,319, 1999.

Finn, C., D. Moore, D. Damaske, and T. Mackey, Aeromagnetic legacy of early subduction along the Pacific margin of Gondwana, *Geology*, *27*, 1087–1090, 1999.

Finn, C., R. E. Bell, D. D. Blankenship, and J. C. Behrendt, The relation of crustal structure, warm mantle, and ice sheets to Cenozoic volcanism in West Antarctica, in *Antarctic Neotectonics*, edited by T. J. Wilson, p. 32, Terra Antarct., Siena, Italy, 2001.

Fitton, J. G., and H. M. Dunlop, The Cameroon Line, West Africa, and its bearing on the origin of oceanic and continental alkali basalt, *Earth Planet. Sci. Lett.*, *72*, 23–38, 1985.

Fitzgerald, P., and S. Baldwin, Detachment fault model for the evolution of the Ross Embayment, in *The Antarctic Region: Geological Evolution and Processes*, edited by C. A. Ricci, pp. 555–564, Terra Antarct., Siena, Italy, 1997.

Fitzgerald, P. G., Thermochronologic constraints on post-Paleozoic tectonic evolution of the central Transantarctic Mountains, Antarctica, *Tectonics*, *13*(4), 818–836, 1994.

Fitzgerald, P. G., and E. Stump, Cretaceous and Cenozoic episodic denudation of the Transantarctic Mountains, Antarctica: New constraints from apatite fission track thermochronology in the Scott Glacier region, *J. Geophys. Res.*, *102*(B4), 7747–7765, 1997.

Fitzgerald, P. G., M. Sandiford, P. J. Barrett, and A. J. W. Gleadow, Asymmetric extension associated with uplift and subsidence in the Transantarctic Mountains and Ross Embayment, *Earth Planet. Sci. Lett.*, *81*, 67–78, 1986.

Foster, D. A., and A. J. W. Gleadow, Reactivated tectonic boundaries and implications for the reconstruction of southeastern Australia and northern Victoria Land, *Geology*, *20*, 267–270, 1992.

Franzini, M., L. Leoni, and M. Saitta, Revisione di una metodologia analitica per fluorescenza-X, basata sulla correzione completa degli effetti di matrice, *Rend. Soc. It. Mineral. Petrol.*, *31*, 365–378, 1975.

Frodeman, R., Geological reasoning: Geology as an interpretive and historical science, *Geol. Soc. Am. Bull.*, *107*, 960–968, 1995.

Gibson, G. M., and T. O. Wright, Importance of thrust faulting in the tectonic development of northern Victoria Land, Antarctica, *Nature*, *315*, 480–483, 1985.

Green, T. H., Petrology and geochemistry of basaltic rocks from the Balleny Is, Antarctica, *Aust. J. Earth Sci.*, *39*, 603–617, 1992.

Halliday, A. N., A. P. Dickin, A. E. Fallick, and J. C. Fitton, Mantle dynamics: A Nd, Sr, Pb and O isotopic study of the Cameroon Line volcanic chain, *J. Petrol.*, *29*, 181–211, 1988.

Halliday, A. N., J. P. Davidson, P. Holden, C. DeWolf, D.-C. Lee, and J. C. Fitton, Trace element fractionation in plumes and the origin of HIMU mantle beneath the Cameroon Line, *Nature*, *347*, 523–528, 1990.

Halliday, A. N., D.-C. Lee, S. Tommasini, G. R. Davies, C. R. Paslick, J. D. Fitton, and D. E. James, Incompatible trace elements in OIB and MORB and source enrichment in the sub-oceanic mantle, *Earth Planet. Sci. Lett.*, *133*, 379–395, 1995.

Hanan, B., and D. Graham, Lead and helium isotope evidence from oceanic basalts for a common deep source of mantle plumes, *Science*, *272*, 991–995, 1996.

Hart, S., J. Blundy, and C. Craddock, Cenozoic volcanism in Antarctica: Jones Mountains and Peter I Island, *Geochim. Cosmochim. Acta*, *59*, 3379–3388, 1995.

Hart, S. R., Heterogeneous mantle domains: signatures, genesis and mixing chronologies, *Earth Planet. Sci. Lett.*, *90*, 273–296, 1988.

Hart, S. R., and P. R. Kyle, Geochemistry of McMurdo Group volcanic rocks, *Antarct. J. U.S.*, *8*(5), 14–16, 1993.

Hart, S. R., E. H. Hauri, L. A. Oschmann, and J. A. Whitehead, Mantle plumes and entrainment: isotopic evidence, *Science*, *256*, 517–520, 1992.

Hart, S. R., J. Blusztanjn, W. E. LeMasurier, and D. C. Rex, Hobbs Coast Cenozoic volcanism: Implications for the West Antarctic rift system, *Chem. Geol.*, *139*, 223–248, 1997.

Hofmann, A. W., *Mantle geochemistry: The message from oceanic volcanism*, 385, 1997.

Hole, M. J., Post-subduction alkaline volcanism along the Antarctic Peninsula, *J. Geol. Soc. London*, *145*, 985–998, 1988.

Hole, M. J., Geochemical evolution of Pliocene-Recent post subduction alkalic basalts from Seal Nunataks, Antarctic Peninsula, *J. Volcanol. Geotherm. Res.*, *40*, 149–167, 1990.

Hole, M. J., and W. E. LeMasurier, Tectonic controls on the geochemical composition of Cenozoic, mafic alkaline volcanic rocks from West Antarctica, *Contrib. Mineral. Petrol.*, *117*, 187–202, 1994.

Hole, M. J., P. D. Kempton, and I. L. Millar, Trace-element and isotopic characteristics of small-degree melts of the asthenosphere: Evidence from the alkalic basalts of the Antarctic Peninsula, *Chem. Geol.*, *109*, 51–68, 1993.

Hole, M. J., A. D. Saunders, G. Rogers, and M. A. Sykes, The relationship between alkaline magmatism, lithospheric extension and slab-window formation along continental destructive plate margins, in *Volcanism Associated With Extension at Consuming Plate Margins*, edited by J. L. Smellie, *Geol. Soc. Spec. Publ.*, *81*, 265–285, 1995.

Kamp, P. J. J., and P. G. Fitzgerald, Geologic constraints on the Cenozoic Antarctica-Australia-Pacific relative plate motion circuit, *Geology*, *15*, 694–697, 1987.

Kyle, P. R., McMurdo Volcanic Group, Western Ross Embayment, in *Volcanoes of the Antarctic Plate and Southern Oceans*, *Antarct. Res. Ser.*, vol. 48, edited by W. E. LeMasurier and J. W. Thomson, pp. 19–25, AGU, Washington, D. C., 1990.

Kyle, P. R., and H. L. Muncy, Geology and geochronology of McMurdo volcanic group rock in the vicinity of Lake Morning, McMurdo Sound, Antarctica, *Antarct. Sci.*, *1*, 345–350, 1989.

Kyle, P. R., W. C. McIntosh, K. S. Panter, and J. L. Smellie, Is volcanism in Marie Byrd Land related to a mantle plume?, in *Sixth International Symposium on Antarctic Earth Sciences*,p. 333, Natl. Inst. of Polar Res., Ranzan-machi, Japan, Sept., 1991.

Kyle, P. R., J. A. Moore, and M. F. Thirlwall, Petrologic evolution of anorthoclase phonolite lavas at Mount Erebus, Ross Island, Antarctica, *J. Petrol.*, *33*, 849–875, 1992.

Lawver, L. A., and L. M. Gahagan, Constraints on timing of extension in the Ross Sea region, *Terra Antarct.*, *1*, 545–552, 1994.

Lawver, L. A., R. J.-Y., D. T. Sandwell, and C. R. Scotese, Evolution of the Antarctic continental margins, in *Geological Evolution of Antarctica*, edited by M. R. A. Thomson, J. A. Crame, and J. V. Thomson, pp. 533–539, Cambridge Univ. Press, New York, 1991.

Lawver, L. A., R. A. Keller, M. R. Fisk, and J. A. Strelin, Bransfield Strait, Antarctic Peninsula: Active extension behind a dead arc, in *Backarc Basins: Tectonics and Magmatism*, edited by B. Taylor, pp. 315–342, Plenum, New York, 1995.

Le Bas, M. J., R. W. Le Maitre, A. Streckeisen, and B. Zanettin, A chemical classification of volcanic rocks based on the total alkali-silica diagram, *J. Petrol.*, *27*, 745–750, 1986.

LeMasurier, W. E., and C. A. Landis, Mantle-plume activity recorded by low relief erosion surfaces in West Antarctica and New Zealand, *Geol. Soc. Am. Bull.*, *108*, 1450–1466, 1996.

LeMasurier, W. E., and D. C. Rex, Evolution of linear volcanic ranges in Marie Byrd Land, Antarctica, *J. Geophys. Res.*, *94*(B6), 7223–7236, 1989.

LeMasurier, W. E., and J. W. Thomson, (Eds.), *Volcanoes of the Antarctic Plate and Southern Oceans*, *Antarct. Res. Ser.*, vol. 48, 487 pp., AGU, Washington, D. C., 1990.

Leoni, L., and M. Saitta, X-ray fluorescence analyses of 29 trace elements in rock and mineral standard, *Rend. Soc. It. Mineral. Petrol.*, *32*, 497–510, 1976.

Lithgow-Bertelloni, C., and M. A. Richards, The dynamics of Cenozoic and Mesozoic plate motions, *Rev. Geophys.*, *36*, 27–78, 1998.

Lucchitta, B. K., J. A. Bowell, and F. Tessensohn, Landsat images for Antarctic research, *Mem. Soc. Geol. It.*, *33*, 35–40, 1987.

McDonough, W. F., and S.-S. Sun, The composition of the Earth, *Chem. Geol.*, *120*, 223–253, 1995.

Minster, J.-F., and C. J. Allègre, Systematic use of trace elements in igneous processes, part III, Inverse problem of batch partial melting in volcanic suites, *Contrib. Mineral. Petrol.*, *68*, 37–52, 1978.

Morgan, W. J., Convection plumes in the lower mantle, *Nature*, *230*, 42–43, 1971.

Müller, P., M. Schmidt-Thomé, H. Kreuzer, F. Tessensohn, and U. Vetter, Cenozoic peralkaline magmatism at the western margin of the Ross Sea, Antarctica, *Mem. Soc. Geol. It.*, *46*, 315–336, 1991.

Orlando, A., S. Conticelli, P. Armienti, and D. Borrini, Experimental study on a basanite from the McMurdo Volcanic Group, Antarctica: inference on its mantle source, *Antarct. Sci.*, *12*, 105–116, 2000.

Panter, K. S., S. R. Hart, P. R. Kyle, J. Blusztanjn, and T. I. Wilch, Geochemistry of Late Cenozoic basalts from the Crary Mountains: Characterization of mantle sources in Marie Byrd Land, Antarctica, *Chem. Geol.*, *165*, 215–241, 2000.

Prestvik, T., C. G. Barnes, B. Sundvoll, and R. A. Duncan, Petrology of Peter I Øy (Peter I Island), West Antarctica, *J. Volcanol. Geotherm. Res.*, *44*, 315–338, 1990.

Richards, M. A., and C. Lithgow-Bertelloni, Plate motion changes, the Hawaii-Emperor bend, and the apparent success and failure of geodynamic models, *Earth Planet. Sci. Lett.*, *137*, 19–27, 1996.

Rocchi, S., S. Tonarini, P. Armienti, F. Innocenti, and P. Manetti, Geochemical and isotopic structure of the early Palaeozoic active margin of Gondwana in northern Victoria Land, Antarctica, *Tectonophysics*, *284*, 261–281, 1998.

Rocchi, S., A. M. Fioretti, and G. Cavazzini, Petrography, geochemistry and geochronology of the Cenozoic Cape Crossfire, Cape King and No Ridge igneous complexes (northern Victoria Land, Antarctica), in *8th International Symposium on Antarctic Earth Sciences Special Volume*, edited by J. A. Gamble, SIR Publ., Wellington, New Zealand, in press, 2002.

Rocholl, A., M. Stein, M. Molzahn, S. R. Hart, and G. Wörner, Geochemical evolution of rift magmas by progressive tapping of a stratified mantle source beneath the Ross Sea Rift, Northern Victoria Land, Antarctica, *Earth Planet. Sci. Lett.*, *131*, 207–224, 1995.

Rossetti, F., F. Storti, and F. Salvini, Cenozoic noncoaxial transtension along the western shoulder of the Ross Sea, Antarctica, and the emplacement of McMurdo dyke arrays, *Terra Nova*, *12*, 60–66, 2000.

Saal, A. E., S. R. Hart, N. Shimizu, E. H. Hauri, and G. D. Layne, Pb isotopic variability in melinclusions from oceanic island basalts, Polynesia, *Science*, *282*, 1481–1484, 1998.

Salvini, F., and F. Storti, Cenozoic tectonic lineaments of the Terra Nova Bay region, Ross Embayment, Antarctica, *Global Planet. Change*, *23*, 129–144, 1999.

Salvini, F., G. Brancolini, M. Busetti, F. Storti, F. Mazzarini, and F. Coren, Cenozoic geodynamics of the Ross Sea region, Antarctica: Crustal extension, intraplate strike-slip faulting, and tectonic inheritance, *J. Geophys. Res.*, *102*(B11), 24,669–24,696, 1997.

Schmidt, D. L., and P. D. Rowley, Continental rifting and transform faulting along the Jurassic Transantarctic Rift, Antarctica, *Tectonics*, *5*, 279–291, 1986.

Sheth, H. C., A historical approach to continental flood basalt volcanism: insights into pre-volcanic rifting, sedimentation, and early alkaline magmatism, *Earth Planet. Sci. Lett.*, *168*, 19–26, 1999.

Sims, K. W. W., and D. J. DePaolo, Inferences about mantle magma sources from incompatible element concentration ratios in oceanic basalts, *Geochim. Cosmochim. Acta*, *61*, 765–784, 1997.

Smith, A. D., and C. Lewis, The planet beyond the plume hypothesis, *Earth Sci. Rev.*, *48*, 135–182, 1999.

Smith, A. G., and D. J. Drewry, Delayed phase change due to hot asthenosphere causes Transantarctic uplift?, *Nature*, *309*, 536–538, 1984.

Stagg, H. M. J., and J. B. Willcox, A case for Australia-Antarctica separation in the Neocomian (ca. 125 Ma), *Tectonophysics*, *210*, 21–32, 1992.

Stern, R. J., U. S. Ten Brink, M. H. P. Bott, Numerical modelling of uplift and subsidence adjacent to the Transantarctic Mountains, in *Recent Progress in Antarctic Earth Science*, edited by Y. Yoshida, K. Kaminuma, and K. Shiraishi, pp. 515–521, TERRAPUB, Tokyo, 1992.

Stern, T. A., and U. S. Ten Brink, Flexural uplift of the Transantarctic Mountains, *J. Geophys. Res.*, *94*(B8), 10,315–10,330, 1989.

Storey, B., P. T. Leat, S. D. Weaver, R. J. Pankhurst, J. D. Bradshaw, and S. Kelley, Mantle plumes and Antarctica-New Zealand rifting: evidence from mid-Cretaceous mafic dykes, *J. Geol. Soc. London*, *156*, 659–671, 1999.

Storey, B. C., and T. Alabaster, Tectonomagmatic controls on Gondwana break-up models: evidence from the proto-Pacific margin of Antarctica, *Tectonics*, *10*(6), 1274–1288, 1991.

Storti, F., F. Rossetti, and F. Salvini, Structural architecture and displacement accommodation mechanisms at the termination of the Priestley Fault, northern Victoria Land, Antarctica, *Tectonophysics*, *341*, 141–161, 2001.

Stump, E., *The Ross Orogen of the Transantarctic Mountains*, 284 pp., Cambridge Univ. Press, New York, 1995.

Stump, E., and P. G. Fitzgerald, Episodic uplift of the Transantarctic Mountains, *Geology*, *20*, 161–164, 1992.

Sun, S. S. and W. F. McDonough, Chemical and isotopic systematics of oceanic basalts: Implications for mantle composition and processes, in *Magmatism in the Ocean Basins*, edited by A. D. Saunders, and M. J. Norry, *Geol. Soc. Spec. Publ.*, *42*, 313–345, 1989.

Tessensohn, F., and G. Wörner, The Ross Sea rift system, Antarctica: Structure, evolution and analogues, in *Geological Evolution of Antarctica: Proceedings of the Fifth International Symposium on Antarctic Earth Sciences*, edited by M. R. A. Thomson, J. A. Crame, and J. W. Thomson, pp. 273–277, Cambridge Univ. Press, New York, 1991.

Tommasi, A., and A. Vauchez, Continental rifting parallel to ancient orogenic belts: An effect of the mechanical anisotropy of the lithospheric mantle, *Earth Planet. Sci. Lett.*, *185*, 199–210, 2001.

Tonarini, S., S. Rocchi, P. Armienti, and F. Innocenti, Constraints on timing of Ross Sea rifting inferred from Cainozoic intrusions from northern Victoria Land, Antarctica, in *The Antarctic Region: Geological Evolution and Processes*, *Proceedings of the 7th International Symposium on Antarctic Earth Sciences*, edited by C. A. Ricci, pp. 511–521, Terra Antarct., Siena, Italy, 1997.

Trey, H., A. K. Cooper, G. Pellis, B. Della Vedova, G. Cochrane, G. Brancolini, and J. Makris, Transect across the West Antarctic rift system in the Ross Sea, Antarctica, *Tectonophysics*, *301*, 61–74, 1999.

Veevers, J. J., Change of tectono-stratigraphic regime in the Australian plate during the 99 Ma (mid-Cretaceous) and 43 Ma (mid-Eocene) swerves of the Pacific, *Geology*, *28*, 47–50, 2000.

Weaver, B. L., The origin of ocean island basalt end-member composition: Trace element and isotopic constraints, *Earth Planet. Sci. Lett.*, *104*, 381–397, 1991.

Wijbrans, J. R., M. S. Pringle, A. A. P. Koppers, and R. Scheveers, Argon geochronology of small samples using the Vulkaan argon laser probe, *Proc. K. Ned. Acad. Wet.*, *98*, 185–218, 1995.

Wilson, J. T., A possible origin of the Hawaiian Islands, *Can. J. Phys.*, *41*, 863–868, 1963.

Wilson, T. J., Cenozoic structural segmentation of the Transantarctic Mountains rift flank in southern Victoria Land, *Global Planet. Change*, *23*, 105–127, 1999.

Wörner, G., L. Vierek, J. Hertoghen, and H. Niephaus, The Mt. Melbourne Volcanic field (Victoria Land, Antarctica), II, Geochemistry and magma genesis, *Geol. Jahrb., Reihe E*, *38*, 395–433, 1989.

Zindler, A., and S. Hart, Chemical geodynamics, *Annu. Rev. Earth Planet. Sci.*, *14*, 493–571, 1986.

P. Armienti, M. D'Orazio, and S. Rocchi, Dipartimento di Scienze della Terra, Università di Pisa, Via S. Maria 53, I-56126 Pisa, Italy. (armienti@dst.unipi.it; dorazio@dst.unipi.it; rocchi@dst.unipi.it)

G. Di Vincenzo and S. Tonarini, Istituto di Geoscienze e Georisorse, CNR, Via Moruzzi, 1, I-56127 Pisa, Italy. (g.divincenzo@igg.cnr.it; s.tonarini@igg.cnr.it)

J. R. Wijbrans, Department of Isotope Geochemistry, Vrije Universiteit, De Boelelaan 1085, NL-1081 Amsterdam, Netherlands. (wijj@geo.vu.nl)